

## First-principles calculation of temperature-composition phase diagrams of semiconductor alloys

S.-H. Wei, L. G. Ferreira, and Alex Zunger

*Solar Energy Research Institute, Golden, Colorado 80401*

(Received 14 August 1989)

The three-dimensional spin- $\frac{1}{2}$  Ising model with multiple-site interactions provides a natural framework for describing the temperature-composition phase diagram of substitutional binary alloys. We have carried out a "first-principles" approach to this problem in the following way: (i) The total energy of an  $A_{1-x}B_x$  alloy in any given substitutional arrangement of  $A$  and  $B$  on a given lattice is expanded in a series of interaction energies  $\{J_f(V)\}$  of "figures"  $f$ . (ii) The  $N_s$  functions  $\{J_f(V)\}$  for "figures"  $f$  are determined as a function of volume  $V$  by equating the total energies of a set of  $N_s$  periodic structures, calculated in the local-density formalism, to a series expansion in  $J_f$  with known coefficients. The calculation includes in a natural way atomic relaxation and self-consistent charge transfer, hence providing a link between the *electronic structure* and the *interaction energies* which decide phase stability. (iii) The number  $N_s$  and range of the interaction energies needed in such an Ising description is determined by the ability of such cluster expansions to reproduce the independently calculated total energy of other structures. We find that this requires extending the expansion for zinc-blende-based alloys up to the fourth fcc neighbors. (iv) Using such a "complete" set of  $N_s$  interaction energies,  $\{J_f\}$ , we find approximate solutions to the corresponding Ising Hamiltonian within the cluster-variation method, retaining up to four-body and fourth-neighbor terms. A renormalization procedure, whereby distant-neighbor correlations are folded into a compact set of *effective* near-neighbor correlations, is used and tested against Monte Carlo solutions. This yields the phase diagram and thermodynamic properties. The set  $\{J_f\}$  is also used to perform a ground-state search of all stable structures. This identifies stable and metastable phases. This approach has been applied to five III-V pseudobinary alloys ( $Al_{1-x}Ga_xAs$ ,  $GaAs_{1-x}P_x$ ,  $In_{1-x}Ga_xP$ ,  $In_{1-x}Ga_xAs$ , and  $GaSb_{1-x}As_x$ ) and three II-VI pseudobinary alloys ( $Cd_{1-x}Hg_xTe$ ,  $Hg_{1-x}Zn_xTe$ , and  $Cd_{1-x}Zn_xTe$ ). We have calculated (i) excess enthalpies, (ii) phase diagrams, (iii) clustering probabilities, and (iv) equilibrium bond lengths. We discuss in detail the chemical trends in these properties and offer a simple (" $\epsilon$ - $G$ ") model which reveals the underlying physical factors controlling such trends.

### I. INTRODUCTION

While recent advances in first-principles formulations of the Born-Oppenheimer total-energy surfaces of crystal lattices<sup>1-6</sup> have produced a wealth of information on the zero-temperature structural properties of solids,<sup>7-11</sup> relatively little has been done in describing with such techniques *temperature-mediated* structural transformations and thermodynamic properties.<sup>12-20</sup> In this paper, we apply our recently formulated "first-principles statistical-mechanics" approach (Ref. 21; hereafter referred to as I) to study composition-temperature phase diagrams of  $A_{1-x}B_x$  substitutional alloys. Here, one considers a given lattice with  $N$  sites, each occupied by either atom  $A$  or atom  $B$  in any one of the  $2^N$  possible configurations  $\sigma$ , and seeks, as a function of temperature  $T$  and composition  $x$ , the phases which minimize the free energy. The excess internal energy  $\Delta E(\sigma, V)$  is expanded in an hierarchical series of volume ( $V$ )-dependent multisite interaction energies,  $\{J_f(V)\}$ , of "figures"  $f$ ; the convergence of the series is established by increasing the number and sizes of such figures. The interaction functions  $\{J_f(V)\}$  are obtained from first-principles self-consistent total-energy calculations on periodic structures

exhibiting various arrangements of atoms  $A$  and  $B$ . The generalized Ising Hamiltonian<sup>22,23</sup> corresponding to the set  $\{J_f(V)\}$  is then solved, finding for each  $(x, T)$  the multisite correlation functions and their thermal averages. These are used to calculate the enthalpy and configurational entropy of the various phases; common-tangent constructions are then used to obtain the phase diagram. Since we are treating alloys which have the fcc structure at *all* compositions, the *excess* vibrational entropy of the alloy relative to its constituents is small<sup>23</sup> and will be neglected here (this is not the case for<sup>23</sup> fcc-bcc alloys). In the present work we apply this approach to study the phase diagrams of a series of tetrahedral face-centered-cubic (fcc) pseudobinary semiconductor alloys  $Al_{1-x}Ga_xAs$ ,  $GaAs_{1-x}P_x$ ,  $In_{1-x}Ga_xP$ ,  $GaSb_{1-x}As_x$ ,  $In_{1-x}Ga_xAs$ ,  $Cd_{1-x}Hg_xTe$ ,  $Hg_{1-x}Zn_xTe$ , and  $Cd_{1-x}Zn_xTe$ . Our objectives are as follows: (i) to establish the extent to which the underlying Hohenberg-Kohn-Sham local-density approximation<sup>1</sup> (LDA) used to obtain the interaction energies  $\{J_f(V)\}$  is capable of describing temperature-mediated configurational phenomena through an Ising model, and (ii) to establish physical trends among tetrahedral semiconductors as pertaining to patterns of order-disorder and phase separation

in their pseudobinary phase diagrams.

In Sec. II we describe the basic methodology of obtaining  $(x, T)$  phase diagrams from volume-dependent total-energy calculations on simple periodic structure. Section III gives results using these volume-dependent Ising energies. Section IV analyzes and explains the chemical trends obtained in terms of a simpler model in which the interaction energies are transformed to a volume-independent set, resulting in the addition to the Hamiltonian of a *global* volume-dependent term. Section V uses this transformed Ising Hamiltonian to search among all possible configurations for ground-state structures. Section VI studies the effects of pressure on the phase diagram. Section VII provides a summary and a classification of all zinc-blende alloys in light of our analysis.

## II. CALCULATING PHASE DIAGRAMS FROM FIRST PRINCIPLES

The method of calculation used here was described in Ref. 21. In this section we give a brief description of the salient features as implemented here.

The excess configurational energy  $\Delta E(\sigma, V)$  for any of the  $2^N$  arrangements  $\sigma$  of atoms  $A$  and  $B$  on a fixed lattice of  $N$  sites is defined with respect to the energy of the pure solids  $A$  and  $B$  at their equilibrium volumes  $V_A$  and  $V_B$ , respectively.  $\Delta E(\sigma, V)$  can be rigorously expanded<sup>24</sup> in an infinite series of multiatom interaction energies  $J_f(V)$  of “figures”  $f$  consisting of  $k$  vertices (the number of sites allowed to interact simultaneously) and up to  $m$  neighbors,

$$\Delta E(\sigma, V) = N \sum_f J_f(V) D_f \bar{\Pi}_f(\sigma), \quad (2.1)$$

where  $\bar{\Pi}_f(\sigma)$  are lattice averages of products of the spins of the figure  $f$  in configuration  $\sigma$  and where  $D_f$  is its degeneracy. Calculation of the phase diagram requires the evaluation of the ensemble average of the excess energy, denoted by angular brackets:

$$\langle \Delta E(V) \rangle = N \sum_f J_f(V) D_f \langle \bar{\Pi}_f \rangle, \quad (2.2)$$

and the configurational entropy for the different possible phases (ordered or disordered) of the alloy. The problem then naturally separates into two parts: (i) “energetics,” i.e., calculation of  $\{J_f(V)\}$  from a microscopic model of  $A$ - $B$  interactions, and (ii) “statistics,” i.e., finding the energy-minimizing correlation functions  $\{\langle \bar{\Pi}_f \rangle\}$ . The free energy, and hence the phase diagram, can be calculated<sup>21–24</sup> from these quantities.

### A. Energetics

Our first approximation is to assume that the series (2.1) converges reasonably rapidly and hence can be truncated at some maximum  $K$ -body,  $M$ -neighbor interaction. This approximation is then examined by the ability of a truncated expansion to reproduce the *directly* calculated total energy of *other* structures  $\sigma' \neq \sigma$ . To the extent that a finite and “small” set of functions,  $\{J_f(V)\}$ , can capture through Eq. (2.1) the essential energetics of arbitrary configurations  $\sigma$  on a given substitutional lattice, we can

determine  $\{J_f(V)\}$  from the total energy of a corresponding set of simple periodic structures.<sup>12</sup> Specializing Eq. (2.1) to such ordered structures  $\{s\}$ , we have

$$\Delta E(s, V) = N \sum_f J_f(V) D_f \bar{\Pi}_f(s). \quad (2.3)$$

The left-hand side of Eq. (2.3) is defined as

$$\Delta E(s, V) = E(A_n B_m, V) - \frac{n}{n+m} E(A_n A_m, V_A) - \frac{m}{n+m} E(B_n B_m, V_B), \quad (2.4)$$

where  $A_n A_m$  or  $B_n B_m$  denote the pure  $A$  and  $B$  solids, respectively. Note, therefore, that the scale of  $\Delta E(s, V)$  is not that of the total energy of a given structure ( $\sim 10^6$  eV for GaAs), or that of the cohesive energy ( $\sim 5$ – $7$  eV for binary semiconductors), but rather the *relative* energy of  $A_n B_m$  with respect to its constituents ( $\sim 10^{-2}$  eV). The large constant terms appearing in  $E(s)$  (e.g., sum of atomic energies) are cancelled in the construct of Eq. (2.4). We calculate  $\Delta E(s, V)$  in the local-density formalism<sup>1</sup> as implemented by the general-potential, linear augmented-plane-wave (LAPW) method.<sup>6</sup> In one case (GaAs-GaP), we have used the first-principles nonlocal pseudopotential method.<sup>3</sup> In either case, the total LDA energy includes kinetic-energy, interelectronic Coulomb, and exchange and correlation terms, as well as the ion-ion and electron-ion interactions:

$$E(s, V) = \sum_{\substack{i \\ (\epsilon_i \lesssim \epsilon_F)}} N_i \epsilon_i - \frac{1}{2} \int \rho(\mathbf{r}) \chi(\mathbf{r}) d\mathbf{r} - \frac{1}{2} \sum_{\alpha} z_{\alpha} V_1(\mathbf{R}_{\alpha}), \quad (2.5a)$$

where

$$\chi(\mathbf{r}) = V_C(\mathbf{r}) + 2[V_{xc}(\mathbf{r}) - \epsilon_{xc}(\mathbf{r})]. \quad (2.5b)$$

Here,  $N_i$  is the occupation number of level  $i$  below the Fermi energy  $\epsilon_F$ ,  $\rho(\mathbf{r})$  is the electronic charge density obtained from the self-consistent single-particle wave functions,  $Z_{\alpha}$  is the atomic number of atom  $\alpha$  at  $\mathbf{R}_{\alpha}$ ,  $V_1(\mathbf{R}_{\alpha})$  is the Coulomb potential at  $\mathbf{R}_{\alpha}$  due to all electrons and nuclei except the charge  $Z_{\alpha}$  at  $\mathbf{R}_{\alpha}$ ,  $V_C$  and  $V_{xc}$  are, respectively, the Coulomb and electronic exchange-correlation potentials, and  $\epsilon_{xc}$  is the exchange-correlation energy density. The Ceperley-Alder exchange-correlation functional as parametrized by Perdew and Zunger<sup>25</sup> was used for GaSb<sub>1-x</sub>As<sub>x</sub> and In<sub>1-x</sub>Ga<sub>x</sub>As in the LAPW calculations and in the pseudopotential calculation; the Hedin-Lundqvist exchange-correlation formula<sup>26</sup> was used for the others. The charge density is determined self-consistently and variationally from the semi-relativistic (i.e., retaining all relativistic terms but spin-orbit interactions) local-density Hamiltonian. For each unit-cell volume  $V$ , we minimize the total energy with respect to the cell-internal atomic coordinates, thereby obtaining relaxed energies. To assure effective numerical cancellation of systematic errors in Eq. (2.4), we use for  $A_n B_m$ ,  $A_n A_m$ , and  $B_n B_m$  precisely equivalent basis sets and integration methods, and sample the Brillouin zone

by sets of wave vectors  $\mathbf{k}$  which are geometrically equivalent in  $A_n B_m$ ,  $A_n A_m$ , and  $B_n B_m$ . We use for the zinc-blende structure the two special  $\mathbf{k}$  points<sup>27(a)</sup> in the LAPW calculation and ten special  $\mathbf{k}$  points in the pseudopotential method; equivalent  $\mathbf{k}$  points are used for all other structures. Convergence tests with respect to  $\mathbf{k}$ -point sampling show that the error in  $\Delta E$  is less than 5 meV per four atoms.<sup>27(b)</sup>

As shown by Connolly and Williams,<sup>12</sup> for a nonsingular  $\det[\bar{\Pi}_f(s)] \neq 0$  in Eq. (2.3), knowledge of  $N_s$  equations of state  $\Delta E(s, V)$  provides the  $N_s$  interaction energy functions

$$J_f(V) = \frac{1}{ND_f} \sum_s^{N_s} [\bar{\Pi}_f(s)]^{-1} \Delta E(s, V). \quad (2.6)$$

This permits expression of the excess energy of *general* configurations  $\sigma$  of Eq. (2.1) as a linear combination of equations of state of periodic structures,

$$\Delta E(\sigma, V) = \sum_s^{N_s} \xi_s(\sigma) \Delta E(s, V), \quad (2.7)$$

where the weights are

$$\xi_s(\sigma) = \sum_f [\bar{\Pi}_f(s)]^{-1} \bar{\Pi}_f(\sigma). \quad (2.8)$$

The key problem is to find a set of structures  $\{s\}$  and figures  $\{f\}$  which affect rapid convergence of Eqs. (2.3) and (2.6). The procedure used is as follows: we select a set of  $N_s$  periodic structures  $\{s\}$ , compute the excess total energies  $\{\Delta E(s, V)\}$  from electronic structure theory [Eqs. (2.4) and (2.5)], and obtain from Eq. (2.6) the  $N_s$  interaction energy functions  $\{J_f(V)\}$ . This set is then used in the series expansion of Eq. (2.3) to predict the total energies  $\{\Delta E(s', V)\}$  for *another* set  $\{s'\} \neq \{s\}$  of periodic structures. This prediction is compared to the *directly* calculated values of  $\Delta E(s', V)$  from electronic-structure theory [e.g., LAPW, see Eqs. (2.4) and (2.5)]. The difference between the energies  $\{\Delta E(s', V)\}$  obtained

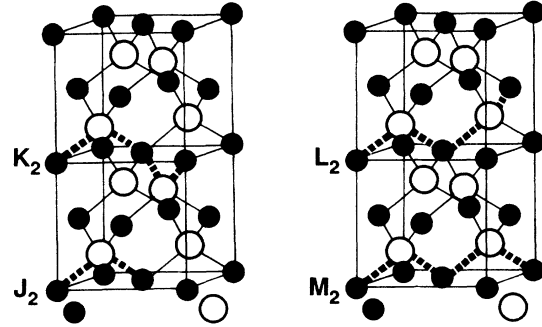


FIG. 1. Schematic depiction of fcc pair interactions between first ( $J_2$ ), second ( $K_2$ ), third ( $L_2$ ), and fourth ( $M_2$ ) neighbors. Note that  $J_2$  passes through a single common sublattice (open circles), while  $K_2$ ,  $L_2$ , and  $M_2$  pass through two  $C$  atoms. More distant neighbor interactions involve three or more  $C$  sites.

from the series-expansion prediction and the “exact” (LAPW) excess energies is then minimized by varying the number and types of figures  $\{f\}$  used in Eq. (2.1), establishing the minimum sizes of  $K$  and  $M$  required to produce a given maximum error we are prepared to tolerate. Our study of isovalent zinc-blende semiconductor alloys in I showed that to achieve a relative error of few percent in  $\Delta E$  requires retention in Eq. (2.1) of up to *fourth fcc neighbors for  $M$  and up to four-body nearest neighbors for  $K$* . These include eight  $J_{k,m}$  terms: (i) a normalization term  $J_{0,1}$ ; (ii) a sites-only term  $J_{1,1}$ ; (iii) four pair-interaction terms  $J_{2,1}$ ,  $J_{2,2}$ ,  $J_{2,3}$ , and  $J_{2,4}$  between first, second, third, and fourth fcc neighbors, respectively (abbreviated in what follows as  $J_2$ ,  $K_2$ ,  $L_2$ , and  $M_2$ , respectively); and (iv) a three-body  $J_{3,1}$  and a four-body  $J_{4,1}$  nearest-neighbor term. Figure 1 depicts by the heavy dashed lines the pair interactions in the fcc unit cell. (Note that what is denoted here as, e.g., “first-nearest neighbors,” refers to first *fcc* neighbors, i.e.,  $A-B$  in  $A_{1-x}B_xC$ ; counting the  $C$  atoms too, this corresponds to second neighbors.) Our study in I has also established an optimal set of structures  $\{s\}$  consistent with the above requirements. Figure 2 depicts these structures, gives their

Ordering Vector	(0,0,0)	(0,0,1)		(2,0,1)	(1,1,1)	
Name	Zincblende (Sphalerite)	Layered tetragonal	“Luzonite”	2 layer superlattice	Chalcopyrite	Layered Trigonal
Formula:	$n = 0,4; AC$	$n = 2; ABC_2$	$n = 1,3; A_3BC_4$	$n = 2; ABC_2$	$n = 2; ABC_2$	$n = 2; ABC_2$
Example: (ternary)	ZnS-type	InGaAs <sub>2</sub> -type (CA)	Cu <sub>3</sub> AsS <sub>4</sub> -type (L1 Or L3)	(AlAs) <sub>2</sub> (GaAs) <sub>2</sub> (Z2)	CuFeS <sub>2</sub> -type (CH)	CrCuS <sub>2</sub> -type (CP)
Bravais Lattice:	Face centered cubic	Simple tetragonal	Simple cubic	Simple tetragonal	Body centered tetragonal	Rhombohedral
Space Group	F $\bar{4}3m$	P $\bar{4}m2$	P $\bar{4}3m$	P $\bar{4}m2$	I $\bar{4}2d$	R $\bar{3}m$
Int. Tables:	F $\bar{4}3m$	P $\bar{4}m2$	P $\bar{4}3m$	P $\bar{4}m2$	I $\bar{4}2d$	R $\bar{3}m$
Schoenflies:	T $_d^2$	D $_{2d}^5$	T $_d^1$	D $_{2d}^5$	D $_{2d}^{12}$	C $_{3v}^5$

FIG. 2. The crystal structures and their space-group notations (in the International Tables and Schoenflies conventions) for the special periodic structures used to obtain the interaction energies. In parentheses we give the abbreviated structure symbols (e.g., CA, CP, and CH) used in the text.

space groups, ordering vectors, Bravais lattices, and the notation used to designate them.

### B. Discussion of the energy expansion

Our formulation of the method of obtaining the interaction energies requires some general comments.

(i) Equation (2.6) shows that  $J_f(V)$  are combinations of *total energies*, i.e., they are not interaction *potentials* often used to fit Born-Oppenheimer energy surfaces.<sup>28</sup> The convergence of a series of interaction *potentials* is often slow, and should not be used to judge the convergence of Eq. (2.1).

(ii) Use of Eq. (2.5) to calculate the total energy of the interacting electron plus nuclear systems avoids the use of the procedure, common in many phase-diagram calculations,<sup>29–32</sup> whereby only the sum of single-particle energies [first term in Eq. (2.5)] is retained. Despite oft-quoted claims<sup>29–35</sup> that the remaining terms of Eq. (2.5) “cancel” (in particular, if charge transfer is “small”), it was never demonstrated, to our knowledge, that useful accuracy [i.e., on the scale of  $\Delta E(\sigma, V)$ ] can be obtained in such an independent-particle scheme.

(iii) In the applications of the Ising model to magnetic interactions,<sup>22</sup> there was no reason to assume that the interaction energies  $\{J_f\}$  depend on internal variables such as magnetization. However, it is obvious that when the endpoint components have different molar volumes  $V_A \neq V_B$ , changing the composition  $x$  (analogous to changing the magnetization) of  $A_{1-x}B_x$  from zero ( $V = V_A$ ) to 1 ( $V = V_B$ ) can change also the alloy volume  $V(x)$ . Since the correlation functions are volume independent, one must represent the volume dependence of the alloy energy,  $\Delta E(\sigma, V)$ , by volume-dependent functions  $J_f(V)$ . We will see that in many cases the volume dependence of  $J_f(V)$  is significant, leading to predictions which depart appreciably from those obtained in a simple Ising model with fixed, volume-independent interactions.

(iv) It was often stated previously in the literature (e.g., Ref. 32) that the excess energy  $\Delta E(\sigma = R, V)$  of a random ( $R$ ) structure cannot be represented as a cluster expansion of the type of Eq. (2.1), and that the energy  $\Delta E(\sigma = s, V)$  of ordered structures  $s$  is unrelated to  $\Delta E(\sigma = R, V)$ . We have shown in I (see Table VII therein) that  $\Delta E(R, V)$  is, in fact, rapidly convergent in terms of a series in  $\{J_f(V)\}$ . Furthermore, specializing Eq. (2.1) to a random structure and substituting from it  $J_{f=0}(V)$  into Eq. (2.3) for an ordered structure  $s$ , one obtains

$$\Delta E[s, V(x)] = \Delta E[R, V(x)] + \sum_{f(\neq 0,1)} [\bar{\Pi}_f(s) - \bar{\Pi}_f(R)] J_f, \quad (2.9)$$

where we have used the property that  $\bar{\Pi}_1(s) = \bar{\Pi}_1(R)$  at the same composition. This establishes the relationship between the energies of random and ordered structures, independent of any perturbation expansion.<sup>31,32</sup> It further shows that while  $\Delta E(R)$  is composition dependent, this does not *require*  $J_{f \geq 2}$  to be composition dependent, as previously thought in the generalized perturbation method (GPM).<sup>31,32</sup>

(v) One might wonder if our procedure of describing the excess energy  $\Delta E(\sigma, V)$  of an alloy in an arbitrary configuration (say, *random*) by constructs obtained from *ordered* structures is likely to be valid, given the often noted<sup>36</sup> differences in the electronic structure of random and ordered alloys of the same composition. Equation (2.9) serves to establish explicitly the terms distinguishing  $\Delta E(s)$  from  $\Delta E(R)$ : the sum of interactions  $J_{f(\neq 0,1)}$  modulated by the difference in correlation functions. Inspection of the observed formation enthalpies<sup>37,38</sup>  $\Delta E(s)$  of ordered intermetallic phases and the mixing enthalpies<sup>39</sup>  $\Delta E(R)$  of the disordered alloy at the same composition shows that while both are typically of order of a few kcal/mol, their difference is often 1 or more order(s) of magnitude smaller. Hence, despite differences in the electronic energy levels (Fermi surfaces, band gaps) of random and ordered compounds, the difference in *integrated* quantities such as total energies tend to be small. This is so since the the dominant  $J_0$  and  $J_1$  terms in the expansion (2.1) are common to both random and ordered phases at the same composition. In all cases studied, we find that the expansion of Eq. (2.9) converges rather rapidly when the correct volume-dependent  $J_f$ s are used.

(vi) Alloys whose constituent atoms have strong chemical interactions or significant size mismatch are known<sup>40</sup> to exhibit “structural relaxation” in the sense that the atomic positions at equilibrium are displaced from “ideal” lattice sites. Such effects are introduced in the present formalism in a natural way by obtaining  $J_f(V)$  from *relaxed* energies  $\Delta E(s, V)$ . We distinguish three forms of relaxation: (a) *Volume relaxation*, whereby the equilibrium alloy volume is determined through establishing  $d\Delta E(\sigma, V)/dV = 0$ . This provides the equilibrium (eq) alloy volume  $V_{\text{eq}}(x, T)$  as well as the equilibrium volumes of ordered phases  $\sigma = s$ . (b) *Cell-internal relaxation* associated with the minimization of  $\Delta E(s, V)$  with respect to the positions of the common sublattice (e.g.,  $C$  in  $A_{1-x}B_xC$ ). In typical semiconductors this relaxation lowers  $\Delta E(s, V_s)$  by<sup>41</sup> up to 80%. (c) *Cell-external relaxation* associated with displacing the mixed ( $A-B$ ) sublattice, e.g., relaxation of the interplanar distances in the CuPt structure or in the  $A_2B_2$  “superlattice” (Fig. 2). This relaxation was found<sup>21</sup> to lower  $\Delta E$  by  $\sim 20\%$ , and substantially alters the phase diagram. All three forms of lattice relaxation are included in the present calculation. Note that in calculations based on the site-coherent-potential approximation<sup>13</sup> (S-CPA), type-(b) and -(c) relaxations are ignored. The same is true for GPM calculations<sup>31,32</sup> and for those<sup>12,14</sup> based on the approach of Connolly and Williams.<sup>12</sup>

(vii) Expansion (2.1) is rigorously correct if all  $2^N$  figures are included;<sup>24</sup> it is approximate if truncated. It is common, in many applications of the Ising model to alloys<sup>12,14,16,22–24,42</sup> to *postulate* the maximum range of interaction, e.g., to retain only the nearest-neighbor term  $J_{2,1}$  or just pair interactions  $J_{2,m}$ ; one then often adjusts  $J_{2,m}$  to fit transition temperatures (e.g., Ref. 42). Our study shows that when  $\{J_f\}$  are calculated from a *microscopic model of electronic interactions*, such truncations are often not warranted. For example, our previous studies of semiconductor-alloy phase diagrams<sup>21</sup> showed that

the series expansion (2.1) departs significantly from convergence if only first-neighbor (“tetrahedron”) interactions ( $M=1$ ) are retained. Such nearest-neighbor models were found<sup>21</sup> to be nonunique and lead to  $\sim 60\%$  errors in miscibility and order-disorder transition temperatures. On the other hand, inclusion of second-, third-, and fourth-neighbor interactions leads to a highly stable representation of all aspects of the fcc phase diagram. Note that calculations based on the CPA (Ref. 13) or on the GPM (Refs. 31 and 32) or the Connolly-Williams approach<sup>12,14</sup> do not provide an *intrinsic* mean of assessing the number of interactions needed to achieve convergence.

### C. Statistics

Having established a self-consistent and practically complete set of interaction-energy functions  $\{J_{k,m}(V)\}$ , one can proceed to calculate the correlation functions and free energy by any of the available methods for calculating the approximate solution of the generalized Ising Hamiltonian [Eq. (2.1)] underlying  $\{J_{k,m}(V)\}$ . The most straightforward method here is the Monte Carlo<sup>43</sup> (MC) method. A more economical method is the tetrahedron cluster-variation method<sup>23,44</sup> (CVM), which provides for fcc systems an excellent approximation to the Monte Carlo method, at a fraction of the computational cost. We refer the reader to Refs. 23 and 44 for a discussion of the CVM (comparison between CVM and MC solutions to the same Ising Hamiltonian is deferred to Sec. IV E). Our calculation here is naturally divided into that for ordered and disordered structures.

#### 1. Statistics for ordered structures

Equation (2.2) gives the average alloy energy in terms of the average product  $\langle \bar{\Pi}_f \rangle$  of the spin variables at the vertices of figure  $f$ . This average represents (i) an ensemble average (denoted by angular brackets), and (ii) an average over equivalent sites in the lattice (denoted by an overbar). An *ordered* structure has generally a lower-symmetry space group than the disordered alloy, and hence sites which were equivalent in the disordered phase need not be equivalent in certain ordered phases. In general, when figures with vertices corresponding to different sublattices must be considered distinct, we have

$$\langle \Delta E(V) \rangle = N \sum_f J_f(V) D_f \langle \Pi_f \rangle, \quad (2.10)$$

where the correlation function  $\langle \Pi_f \rangle$  (without an overbar) has been redefined with respect to the ordered space group. The variational value of the free energy,  $\Delta F = \Delta E - T \Delta S$ , is searched by minimizing it simultaneously with respect to all  $\{\langle \Pi_f \rangle\}$ , i.e.,  $\partial \Delta F / \partial \langle \Pi_f \rangle = 0$ . This is done in practice using a Newton iteration scheme<sup>45</sup> (limiting, however, the steps in  $\langle \Pi_f \rangle$  so that the reduced density matrix<sup>46</sup> remains positive at each step). More details are given in Refs. 24, 44, 45, and 47.

The basic remaining question is how many figures should be used for the *energy* expansion in Eq. (2.10) and for the *entropy* expansion<sup>46</sup> (the two need not be the same). In paper I we have addressed the first question, finding that for fcc semiconductors one needs to include in Eq. (2.10) figures up to fourth-nearest-neighbor pairs (eight figures). This was decided on the basis of *energy-convergence* tests (Tables V and VII in paper I). Naively, one would have guessed that the same figures should be used in evaluating the *entropy* term. However, previous calculations<sup>48</sup> suggest but small (and irregular) changes in  $\Delta S$  as the figures used to calculate it extend beyond a tetrahedron. In fact, the tetrahedron approximation provides excellent estimates of the configurational entropy as calculated by accurate Monte Carlo simulations; see Fig. 15 below. We hence calculate the entropy by limiting the correlation functions to a nearest-neighbor tetrahedron. This strategy of extending  $\{f\}$  for energy calculations beyond the limit used for entropy calculations is executed by our renormalization procedure,<sup>21</sup> whereby higher-order correlations are folded into tetrahedron correlations. This leads us to our second approximation (the first was discussed in Sec. II A): If a figure has two spin variables separated by a distance larger than some critical distance  $d_{\text{stat}}$ , they will be assumed to be *statistically uncorrelated*. Hence, if a figure  $\phi$  has sites  $\alpha, \beta, \dots, \omega$  and  $\Pi_\phi = \hat{S}_\alpha \hat{S}_\beta \cdots \hat{S}_\omega$ , we will assume

$$\langle (\hat{S}_\alpha - q_\alpha)(\hat{S}_\beta - q_\beta) \cdots (\hat{S}_\omega - q_\omega) \rangle = 0 \quad (2.11)$$

if  $\phi$  is outside the range  $d_{\text{stat}}$ , where  $q_\alpha = \langle \hat{S}_\alpha \rangle$ . Using  $d_{\text{stat}} = \text{first-neighbor distance}$ , this leads for ordered structures to

$$\langle \Pi_{2,m} \rangle = \langle \Pi_{1,1} \rangle \langle \Pi_{1',1} \rangle, \quad (2.12)$$

for  $m > 1$  as proposed by Morita.<sup>47</sup> Here the vertex labeled  $1'$  may belong to a different sublattice than the vertex labeled  $1$ . Note that as  $T \rightarrow 0$  and the partially ordered structures become perfectly ordered, the point correlation functions  $\langle \Pi_{1,1} \rangle$  and  $\langle \Pi_{1',1} \rangle$  become either  $+1$  (if the sublattice has atoms  $B$ ) or  $-1$  (if  $A$ ), and so does the pair correlation  $\langle \Pi_{2,m} \rangle$ . In this case the average in the fcc lattice,  $\langle \bar{\Pi}_{2,m} \rangle$  (note the overbar), calculated in Eq. (2.12) reduces to the  $\bar{\Pi}_{2,m}$  of the perfectly ordered phases. When  $T \rightarrow \infty$  the sublattices become equivalent and  $\langle \bar{\Pi}_{2,m} \rangle$  reduces to  $(2x - 1)^2$ .

#### 2. Statistics for the disordered phase: The renormalized interaction approach

Our basic approximation of Eq. (2.11) for renormalization of distant-neighbor correlations led to Eq. (2.12) for *ordered* structures. For the high-symmetry disordered phase,  $q_\alpha$  of Eq. (2.11) is simply  $2x - 1$ ; hence, for  $m > 1$ ,

$$\langle \Pi_{2,m} \rangle = \langle \Pi_{1,1} \rangle^2 = (2x - 1)^2. \quad (2.13)$$

This leads to a simple renormalization of the distant-neighbor interaction energies, whereby the volume-

dependent set  $\{J_f(V)\}$  transforms into a volume- and composition-dependent set  $\{\tilde{J}_g(x, V)\}$ . While  $\{J_f(V)\}$  has figures  $\{f\}$  extending beyond  $d_{\text{stat}}$  (e.g., to fourth pair interactions), the set  $\{\tilde{J}_g(x, V)\}$  is limited to  $g$  within the range  $d_{\text{stat}}$  (i.e., in our example to first neighbors, i.e., five  $g$  values), and folds figures with  $f > g$  into the set  $\{g\}$ :

$$\tilde{J}_g(x, V) = J_g(V) + \sum_{f(>g)} A_f(x) J_f(V). \quad (2.14)$$

The ensemble-average energy for the disordered phase [Eq. (2.10)] then becomes

$$\Delta E \langle (V) \rangle = N \sum_k D_{k,1} \tilde{J}_{k,1}(x, V) \langle \bar{\Pi}_{k,1} \rangle, \quad (2.15)$$

where the sum extends only to figures within  $d_{\text{stat}}$ , i.e., here to a nearest-neighbor tetrahedron.

It is useful to define<sup>21</sup> the *effective equations of state*  $\bar{\epsilon}_k(\{P_k\}, V)$  which depend on composition and temperature through the probabilities  $P_k = P_k(x, T)$ . We found in practical applications<sup>21</sup> that this temperature dependence is negligible in the range  $0 < T < 40\,000$  K; hence, replacing the variational  $P_k(x, T)$  by the value  $P_k(x, \infty)$  appropriate to the random alloy introduces numerically insignificant errors in the phase diagram. Explicit equations are given in Eqs. (6.15)–(6.16) of Ref. 21. These effective equations of state can be used to express the ensemble average of the total energy, Eq. (2.15), as<sup>21</sup>

$$\langle \Delta E(\sigma, V) \rangle = \sum_n P_n \bar{\epsilon}_n(x, V), \quad (2.16)$$

where  $P_n$  are the effective probabilities of finding cluster  $n$ .

Neglecting distant-neighbor interactions  $J_{f>g} = 0$  in Eq. (2.14) gives the simple first-nearest-neighbor model used in many previous applications of the Ising model to alloys.<sup>12,14,16,22,23</sup> Using Eqs. (2.13)–(2.16) instead, we include further-neighbor interactions without introducing any major complication over the nearest-neighbor model.

It is interesting to observe how the inclusion of distant-neighbor interactions modifies the equations of state  $\bar{\epsilon}_{k,1}(V)$  relative to the five simple first-nearest-neighbor *unnormalized* equations of state  $\Delta E(n, V)$ . For this purpose it is useful to represent both by the same analytic form,

$$\begin{aligned} \bar{\epsilon}_n(V) &= \Delta \bar{H}_n + f[\bar{V}_n, \bar{B}_n, \bar{B}'_n], \\ \Delta E(n, V) &= \Delta H_n + f[V_n, B_n, B'_n], \end{aligned} \quad (2.17)$$

where the equilibrium energies are  $\Delta \bar{H}_n$  and  $\Delta H_n$ , respectively, and  $[\bar{V}_n, \bar{B}_n, \bar{B}'_n]$  and  $[V_n, B_n, B'_n]$  are the equilibrium volume, bulk modulus, and the latter's pressure derivative; values with an "overtilde" denote results obtained with renormalized interactions. This comparison is given and discussed in Sec. III G.

While intuitively appealing, our second approximation of Eq. (2.11) requires demonstration. In Sec. IV E we

compare the phase diagram calculated with the CVM and folded interactions to that obtained from a Monte Carlo simulation on the same Hamiltonian, but retaining  $J_{2,2}$ ,  $J_{2,3}$ , and  $J_{2,4}$  without folding. The results show that virtually no precision is lost by the folding procedure.

### III. RESULTS

This section describes the phase diagrams and thermodynamic properties obtained from the Ising model with volume-dependent interaction energies.

#### A. $\Delta E(s, V)$ for the ordered structures

Table I gives for each of the eight alloy systems studied the calculated equilibrium lattice constants, cell-internal relaxation parameter  $u$ , and the formation enthalpy  $\Delta E(s, V_s) \equiv \Delta H_s$  of the eight periodic structures of Fig. 2.

The results can be classified into two groups: those for the nearly-lattice-matched alloys (AlAs-GaAs and CdTe-HgTe) and those for the lattice-mismatched alloys (all the rest).

For the lattice-matched structures, we find the order of formation enthalpies

$$\Delta H(\text{CA}) > \Delta H(\text{CH}) > \Delta H(\text{CP}) > \Delta H(\text{Z2}), \quad (3.1)$$

whereas for the lattice-mismatched systems we find

$$\Delta H(\text{CP}) > \Delta H(\text{CA}) \simeq \Delta H(\text{Z2}) > \Delta H(\text{CH}) \quad (3.2)$$

(the structure symbols CP, CA, Z2 and CH are defined in Fig. 2). The order in the first sequence has been previously explained<sup>20</sup> in terms of the electrostatic energies of these lattices at fixed volume, whereas the order in the second sequence has been shown to reflect the ability of the different lattices to reduce the strain energy associated with atomic-size mismatch through structure-dependent relaxation patterns.

Lattice-matched systems exhibit little structural relaxation ( $u \simeq \frac{1}{4}$  in Table I), whereas lattice-mismatched systems show significant relaxation, leading to dissimilar  $A-C$  and  $B-C$  bond lengths. The equilibrium lattice constants tend to be linear with composition, and exhibit a very weak dependence on the crystal structure for fixed compositions.

For all of the six ternary structures studied in the eight alloy systems, we find

$$\Delta E(s, V_s) \equiv \Delta H_s > 0, \quad (3.3)$$

i.e., a phase-separated  $AC + BC$  systems is lower in energy than any of these ordered structures. In recent work,<sup>49</sup> however, we find  $\Delta H(\text{AlInP}_2) < 0$  in the chalcopyrite structure.

Other total-energy calculations exist in the literature<sup>50–55</sup> for a few of the compounds studied here. The results are compared in Table II (Refs. 50–55) for the

TABLE I. Calculated equilibrium lattice parameters  $a$ , cell-internal relaxation parameters  $\mu$ , and formation enthalpy  $\Delta H$  for the eight ordered structures of Fig. 2. All the results are LAPW calculations using the equivalent of two special zinc-blende  $k$  points in the Brillouin-zone sampling (Ref. 27), except for  $\text{GaAs}_4\text{-P}_n$ , which are calculated using pseudopotential methods with  $E_1 = 15$  Ry cutoff energy, the equivalent of 10 special zinc-blende  $k$  points and the correlation of Ref. 25. This correlation was also used in the LAPW calculation for  $\text{InGaAs}$  and  $\text{GaAsSb}$ ; other LAPW calculations used the correlation of Ref. 26. We also give the substitution energy  $\epsilon^{(s)}$  of Eq. (4.4), discussed in Sec. IV B. The two values for the relaxation parameter  $\mu$  in the CP and Z2 structures correspond to the two independent  $A-C$  (and two  $B-C$ ) bonds.

Compound	Struct.	$a$ (Å)	$\mu$	$\Delta H_s$ (meV/four- atoms)	$\epsilon^{(s)}$ (meV/four- atoms)	Compound	Struct.	$a$ (Å)	$\mu$	$\Delta H_s$ (meV/four- atoms)	$\epsilon^{(s)}$ (meV/four- atoms)
$\text{AlAs}$	ZB	5.6569	0.25	0.0	0.0	$\text{InAs}$	ZB	6.0838	0.25	0.0	0.0
$\text{Al}_3\text{GaAs}_4$	L1	5.6569	0.25	8.7	8.7	$\text{In}_3\text{GaAs}_4$	L1	5.9833	0.2402	51.7	-108.82
$\text{AlGaAs}_2$	CP	5.6569	0.25	7.5	7.5	$\text{InGaAs}_2$	CP	5.8827	0.2414	108.5	-114.50
			0.25						0.2585		
$\text{AlGaAs}_2$	CA	5.6569	0.25	11.5	11.5	$\text{InGaAs}_2$	CA	5.8827	0.2304	66.7	-156.30
$\text{AlGaAs}_2$	Z2	5.6569	0.25	2.85	2.85	$\text{InGaAs}_2$	Z2	5.8827	0.25	62.4	-160.60
			0.25						0.2304		
$\text{AlGaAs}_2$	CH	5.6569	0.25	9.8	9.8	$\text{InGaAs}_2$	CH	5.8827	0.2278	16.5	-206.50
$\text{AlGa}_3\text{As}_4$	L3	5.6569	0.25	8.4	8.4	$\text{InGa}_3\text{As}_4$	L3	5.7822	0.2597	62.4	-112.08
$\text{GaAs}$	ZB	5.6569	0.25	0.0	0.0	$\text{GaAs}$	ZB	5.6816	0.25	0.0	0.0
$\text{GaAs}$	ZB	5.613	0.25	0.0	0.0	$\text{CdTe}$	ZB	6.470	0.25	0.0	0.0
$\text{Ga}_4\text{As}_3\text{P}$	L1	5.561	0.2450	10.5	-31.87	$\text{Cd}_3\text{HgTe}_4$	L1	6.476	0.2505	7.4	7.0
$\text{Ga}_7\text{AsP}$	CP	5.510	0.2465	37.2	-30.17	$\text{CdHgTe}_2$	CP	6.481	0.2504	9.8	9.3
			0.2560						0.2496		
$\text{Ga}_2\text{AsP}$	CA	5.510	0.2415	26.6	-40.77	$\text{CdHgTe}_2$	CA	6.481	0.2515	12.1	11.6
$\text{Ga}_7\text{AsP}$	Z2	5.510	0.25	24.3	-43.07	$\text{CdHgTe}_2$	Z2	6.481	0.25	4.7	4.2
			0.2415						0.2515		
$\text{Ga}_7\text{AsP}$	CH	5.510	0.2384	6.5	-60.87	$\text{CdHgTe}_2$	CH	6.481	0.2518	11.3	10.8
$\text{Ga}_4\text{AsP}_3$	L3	5.458	0.2548	19.8	-39.0	$\text{CdHg}_3\text{Te}_4$	L3	6.485	0.2496	10.4	10.2
$\text{GaP}$	ZB	5.406	0.25	0.0	0.0	$\text{HgTe}$	ZB	6.492	0.25	0.0	0.0
$\text{InP}$	ZB	5.9183	0.25	0.0	0.0	$\text{HgTe}$	ZB	6.492	0.25	0.0	0.0
$\text{In}_3\text{GaP}_4$	L1	5.8015	0.2383	51.3	-168.97	$\text{Hg}_3\text{ZnTe}_4$	L1	6.383	0.2393	26.9	-124.54
$\text{InGaP}_2$	CP	5.6943	0.2369	155.4	-166.02	$\text{HgZnTe}_2$	CP	6.269	0.2388	103.3	-106.07
			0.2630						0.2613		
$\text{InGaP}_2$	CA	5.6905	0.2257	91.0	-230.42	$\text{HgZnTe}_2$	CA	6.269	0.2279	42.5	-166.87
$\text{InGaP}_2$	Z2	5.6905	0.25	95.0	-226.42	$\text{HgZnTe}_2$	Z2	6.269	0.25	46.5	-162.87
			0.2217						0.2279		
$\text{InGaP}_2$	CH	5.6857	0.2217	19.0	-302.42	$\text{HgZnTe}_2$	CH	6.269	0.2260	11.4	-197.97
$\text{InGa}_3\text{P}_4$	L3	5.5771	0.2633	82.95	-179.66	$\text{HgZn}_3\text{Te}_4$	L3	6.163	0.2611	36.4	-125.85
$\text{GaP}$	ZB	5.4616	0.25	0.0	0.0	$\text{ZnTe}$	ZB	6.052	0.25	0.0	0.0

TABLE I. (Continued).

Compound	Struct.	$a$ (Å)	$u$	$\Delta H_s$ (meV/four- atoms)	$\epsilon^{(s)}$ (meV/four- atoms)	Compound	Struct.	$a$ (Å)	$u$	$\Delta H_s$ (meV/four- atoms)	$\epsilon^{(s)}$ (meV/four- atoms)
GaSb	ZB	6.1068	0.25	0.0	0.0	CdTe	ZB	6.470	0.25	0.0	0.0
Ga <sub>4</sub> Sb <sub>3</sub> As	L1	6.0071	0.2417	88.0	-80.3	Cd <sub>3</sub> ZnTe <sub>4</sub>	L1	6.368	0.2397	33.0	-100.53
Ga <sub>2</sub> SbAs	CP	5.8974	0.2410	132.0	-104.66	CdZnTe <sub>2</sub>	CP	6.263	0.2393	103.5	-81.11
			0.2590						0.2608		
Ga <sub>2</sub> SbAs	CA	5.8927	0.2336	115.0	-121.66	CdZnTe <sub>2</sub>	CA	6.263	0.2290	54.2	-130.41
Ga <sub>2</sub> SbAs	Z2	5.8927	0.25	97.0	-139.66	CdZnTe <sub>2</sub>	Z2	6.263	0.25	59.4	-154.91
			0.2336						0.2290		
Ga <sub>2</sub> SbAs	CH	5.8922	0.2294	52.0	-184.66	CdZnTe <sub>2</sub>	CH	6.263	0.2271	19.2	-165.41
Ga <sub>4</sub> SbAs <sub>3</sub>	L3	5.7852	0.2579	100.0	-87.30	CdZn <sub>3</sub> Te <sub>4</sub>	L3	6.158	0.2609	46.9	-96.62
GaAs	ZB	5.6816	0.25	0.0	0.0	ZnTe	ZB	6.052	0.25	0.0	0.0

binary constituents where experimental data<sup>56</sup> is also included and in Table III for the  $ABC_2$  CuAu-I structure. Note that pseudopotential calculations<sup>50-55</sup> tend to produce systematically smaller equilibrium lattice constants for binary semiconductors with  $d$ -shell cations than do the all-electron (e.g., LAPW) approaches. The difference is substantial in systems where the anion valence  $p$ -orbital energy is close to the highest occupied cation  $d$ -orbital energy (e.g., HgTe). The origins of this effect is probably the absence of  $p$ - $d$  repulsion in the pseudopotential representation, and this was discussed in detail in Ref. 57. Our calculated excess energies for the CuAu-I structure (Table III) are systematically lower than that obtained by Boguslawski and Baldereschi,<sup>51</sup> while the relaxation parameters and the strain energies of the binary constituents are similar. We attribute the former difference to a better convergence in basis functions in the present (all-electron) calculation. Our results for AlGaAs<sub>2</sub> are close to those of Bylander and Kleinman,<sup>54</sup> for InGaAs<sub>2</sub> to those of Ohno,<sup>52</sup> and for Ga<sub>2</sub>SbAs to those of Qteish *et al.*<sup>53</sup> The results of Nelson and Batra<sup>50</sup> for InGaP<sub>2</sub> are significantly different, presumably due to poor convergence.

For convenience of calculation, we have fitted each  $\Delta E(s, V)$  to a volume-dependent (Murnaghan)<sup>58,59</sup> equation of state whose parameters are  $B_s$  and  $B'_s$  (the bulk modulus and its pressure derivative, respectively), and  $V_s$  (the equilibrium volume). In the course of the work described in I, we found that the numerical errors associated with obtaining high derivatives of  $\Delta E(s, V)$  (i.e.,  $B_s$  and  $B'_s$ ) for the ternary compounds can be as large as  $\sim 10\%$  for  $B_s$  and even larger for  $B'_s$ , leading to an  $\sim 5\%$  uncertainty in the calculated miscibility gap. Calculation of the phase diagram for a prototype system (GaAs-GaSb) showed<sup>21</sup> that use of the concentration-weighted linearized quantities

$$V_n = (1 - X_n)V_{AC} + X_n V_{BC} ,$$

$$B_n = (1 - X_n)B_{AC} + X_n B_{BC} , \quad (3.4)$$

$$B'_n = (1 - X_n)B'_{AC} + X_n B'_{BC} ,$$

where  $X_n$  is the fraction of  $B$  atoms in the ordered structure, produced results that are within the range obtained from  $\Delta E(s, V)$  with numerically computed  $\{V_s, B_s, B'_s\}$ , given the error in the latter. We hence judge approximation (3.4) to be both useful (since it requests a full volume scan only for  $AC$  and  $BC$ , and only a limited scan, near equilibrium, for the intermediate compounds) and sufficiently accurate ( $\sim 5\%$  in miscibility temperature). It is important to note that while  $\{V_s, B_s, B'_s\}$  are linearized for the *ordered* structures, the formation enthalpies  $\Delta H_s$  are not linearized, as they obviously exhibit significant deviation from zero.

The first three columns of Tables IV and V give the calculated  $V_s$ ,  $B_s$ , and  $B'_s$  values for the eight semiconductor systems studied here; Table I gives  $\Delta H_s$ . This defines the full input to the phase-diagram calculations.

TABLE II. Comparison of the calculated equilibrium lattice constants (in Å) of the zinc-blende semiconductors discussed in this study, as obtained from various nonlocal first-principles pseudopotential (ps) and all-electron (AE) implementations of the local-density formalism. For comparison, low-temperature experimental values are also shown. References below indicate the basis-set cutoff ( $E_1$ ) and type of exchange correlation (xc) used in each case.

	a (ps)	b (ps)	c (ps)	d (ps)	e (ps)	f (ps)	g (ps)	Present LAPW (AE)	Expt. <sup>h</sup>
AlAs						5.6696		6.657	5.662
GaP	5.31	5.406	5.34					5.462	5.451
GaAs		5.613	5.57	5.572	5.56	5.6548		5.682	5.653
GaSb			6.01		5.96			6.107	6.096
InP	5.60		5.75					5.918	5.869
InAs			5.95	5.905				6.084	6.058
ZnTe							5.618	6.052	6.089
CdTe							5.818	6.470	6.481
HgTe							5.616	6.492	6.461

<sup>a</sup>Reference 50,  $E_1 = 10$  Ry, 48 superlattice  $\mathbf{k}$  points, Wigner xc.

<sup>b</sup>Present pseudopotential study,  $E_1 = 15$  Ry, 10  $\mathbf{k}$  points, Ceperley-Alder xc.

<sup>c</sup>Reference 51, pseudopotential,  $E_1 = 12$  Ry, two  $\mathbf{k}$  points, Ceperley-Alder xc.

<sup>d</sup>Reference 52, pseudopotential,  $E_1 = 13$  Ry, 12 superlattice  $\mathbf{k}$  points, Wigner xc.

<sup>e</sup>Reference 53, pseudopotential,  $E_1 = 12$  Ry, two  $\mathbf{k}$  points, Ceperley-Alder xc.

<sup>f</sup>Reference 54, Gaussian basis, 12  $\mathbf{k}$  points, Wigner xc.

<sup>g</sup>Reference 55, pseudopotential,  $E_1 = 8$  Ry, two  $\mathbf{k}$  points, Hedin-Lundqvist xc.

<sup>h</sup>Reference 56.

TABLE III. Calculated formation enthalpies  $\Delta H$  (in meV/four-atoms) of the  $n=1$  (001) superlattice (the CuAu-I-like structure) using pseudopotential (ps) and the present all-electron (AE) implementations of the local-density formalism [Ref. 27(b)]. We also show the cell-internal distortion parameters  $u$  and the “constituent strain energies,” i.e., the energy  $\Delta E_{cs}$  of the binary constituents constrained in the parallel dimension to a substrate  $a_s$  (and relaxed in the perpendicular dimension). Note that  $\Delta H - \Delta E_{cs}$  is the “epitaxial formation enthalpy”  $\delta H$  (see Ref. 41). This quantity was found to be positive for GaInP<sub>2</sub> and GaInAs<sub>2</sub> in the ps calculations of Ref. 51, but it is close to zero or negative in the present AE calculation. References pertain to the notation of Table II.

	$a_{sq}$ (Å)	$u$ or $u - \frac{1}{2}$	$\Delta H$ (meV/four-atoms)	Ref.
GaAlAs <sub>2</sub>	5.6622	$\frac{1}{4}$	15.1	a
	5.6569	$\frac{1}{4}$	11.5	present
GaInP <sub>2</sub>	5.45	0.2317	54.4	b
	5.530	0.23	115.6	c
	5.6905	0.2257	91.0	present
GaInAs <sub>2</sub>	5.756	0.233	83.6	c
	5.701	0.234	60.1	d
	5.883	0.230	66.7	present
Ga <sub>2</sub> AsSb	5.812	0.234	129.2	c
	5.76	0.234	114.8	e
	5.8927	0.2336	115.0	present
GaP + InP on $a_s$	$a_s = 5.53$		102.8	c
	$a_s = 5.6905$		98.0	present
GaAs + InAs on $a_s$	$a_s = 5.76$		54.0	c
	$a_s = 5.70$		53.4	d
	$a_s = 5.883$		72.1	present
GaAs + GaSb on $a_s$	$a_s = 5.81$		81.2	c
	$a_s = 5.893$		80.0	present

<sup>a</sup>Reference 54.

<sup>b</sup>Reference 50.

<sup>c</sup>Reference 51.

<sup>d</sup>Reference 52.

<sup>e</sup>Reference 53.

TABLE IV. Calculated values of the equilibrium molar volumes  $V_n$ , the bulk moduli  $B_n$ , and their pressure derivatives  $B'_n$  for III-V alloys. Values in parentheses are interpolated as indicated in Eq. (3.4). Also given are the values deduced from the renormalized equations of state, indicated with an overtilde (see Sec. III G).

Compound	$V_n$ (cm <sup>3</sup> /mol)	$B_n$ (GPa)	$B'_n$	$\tilde{V}_n$ (cm <sup>3</sup> /mol)	$\tilde{B}_n$ (GPa)	$\tilde{B}'_n$	$\Delta\tilde{H}_n$ (meV/four-atoms)
AlAs	27.254	74.0	5.0	27.254	74.0	5.0	0.0
Al <sub>3</sub> GaAs <sub>4</sub>	27.254	74.0	5.0	27.254	74.0	5.0	6.68
AlGaAs <sub>2</sub>	27.254	74.0	5.0	27.254	74.0	5.0	8.85
AlGa <sub>3</sub> As <sub>4</sub>	27.254	74.0	5.0	27.254	74.0	5.0	6.42
GaAs	27.254	74.0	5.0	27.254	74.0	5.0	0.0
GaAs	26.631	75.6	4.0	26.631	56.31	4.13	0.0
Ga <sub>4</sub> As <sub>3</sub> P	(25.920)	(78.275)	(4.0)	25.917	58.69	4.07	0.00
Ga <sub>2</sub> AsP	(25.209)	(80.950)	(4.0)	25.205	61.02	4.01	12.49
Ga <sub>4</sub> AsP <sub>3</sub>	(24.498)	(83.625)	(4.0)	24.495	63.30	3.95	9.02
GaP	23.787	86.3	4.0	23.787	65.52	3.89	0.0
InP	31.209	68.70	4.31	31.209	52.40	2.03	0.0
In <sub>3</sub> GaP <sub>4</sub>	(29.538)	(72.875)	(4.38)	39.500	53.61	2.23	11.54
InGaP <sub>2</sub>	(27.868)	(77.050)	(4.45)	27.811	54.62	2.45	34.53
InGa <sub>3</sub> P <sub>4</sub>	(26.197)	(81.225)	(4.52)	26.150	55.40	2.65	37.40
GaP	24.527	85.40	4.59	24.527	55.86	2.87	0.0
GaSb	34.287	51.8	6.78	34.287	36.08	8.15	0.0
Ga <sub>4</sub> Sb <sub>3</sub> As	(32.619)	(57.5)	(6.54)	32.590	40.61	6.17	48.94
Ga <sub>2</sub> SbAs	(30.951)	(63.2)	(6.30)	30.887	43.64	4.03	60.57
Ga <sub>4</sub> SbAs <sub>3</sub>	(29.283)	(68.9)	(6.06)	29.205	44.56	1.37	56.05
GaAs	27.615	74.6	5.82	27.615	36.08	-2.45	0.0
InAs	33.905	58.70	4.15	33.905	44.07	-0.79	0.0
In <sub>3</sub> GaAs <sub>4</sub>	(32.332)	(62.68)	(4.57)	32.288	44.74	1.27	21.95
InGaAs <sub>2</sub>	(30.760)	(66.65)	(4.99)	30.714	46.42	3.63	24.56
InGa <sub>3</sub> As <sub>4</sub>	(29.187)	(70.63)	(5.40)	29.168	48.98	6.21	29.42
GaAs	27.615	74.60	5.82	27.615	52.52	8.83	0.0

TABLE V. Calculated values of the equilibrium molar volumes  $V_n$ , the bulk moduli  $B_n$ , and their pressure derivatives  $B'_n$  for II-IV alloys. Values in parentheses are interpolated as indicated in Eq. (3.4). Also given are the values deduce from the renormalized equations of state, indicated with an overtilde (see Sec. III G).

Compound	$V_n$ (cm <sup>3</sup> /mol)	$B_n$ (GPa)	$B'_n$	$\tilde{V}_n$ (cm <sup>3</sup> /mol)	$\tilde{B}_n$ (GPa)	$\tilde{B}'_n$	$\Delta\tilde{H}_n$ (meV/four-atoms)
CdTe	40.776	44.00	4.40	40.776	45.0	4.5	0.0
Cd <sub>3</sub> HgTe <sub>4</sub>	(40.880)	(44.53)	(4.45)	40.881	45.0	4.5	10.06
CdHgTe <sub>2</sub>	(40.985)	(45.05)	(4.50)	40.985	45.0	4.5	11.63
CdHg <sub>3</sub> Te <sub>4</sub>	(41.089)	(45.58)	(4.55)	41.089	45.0	4.5	6.85
HgTe	41.193	46.10	4.60	41.193	45.0	4.5	0.0
HgTe	41.193	46.1	4.60	41.193	34.77	0.91	0.0
Hg <sub>3</sub> ZnTe <sub>4</sub>	(39.238)	(47.6)	(4.65)	39.177	33.48	0.75	11.19
HgZnTe <sub>2</sub>	(37.283)	(49.1)	(4.70)	37.184	31.88	0.47	17.87
HgZn <sub>3</sub> Te <sub>4</sub>	(35.328)	(50.6)	(4.75)	35.235	29.99	0.09	15.53
ZnTe	33.373	52.1	4.80	33.373	27.90	-0.45	0.0
CdTe	40.776	44.00	4.40	40.776	35.55	1.19	0.0
Cd <sub>3</sub> ZnTe <sub>4</sub>	(38.925)	(46.03)	(4.50)	38.884	35.47	1.49	16.05
CdZnTe <sub>2</sub>	(37.074)	(48.05)	(4.60)	37.015	35.36	1.83	29.33
CdZn <sub>3</sub> Te <sub>4</sub>	(35.224)	(50.08)	(4.70)	35.176	35.21	2.21	26.55
ZnTe	33.373	52.10	4.80	33.373	34.99	2.65	0.0

### B. Multiatom interaction energies $J_f(V)$

Using  $\{\Delta E(s, V)\}$  for the eight special periodic structures (Fig. 2) and Eq. (2.6), we obtain the volume-dependent interaction energies depicted in Fig. 3 for three alloy systems. These show the following.

(i)  $J_0(V)$  and  $J_1(V)$  have a significant volume dependence;  $J_0(V)$  is much larger at  $x = \frac{1}{2}$  than all  $J_{f \neq 0}$ . Many applications of the Ising model to alloy phase diagrams<sup>22,23,29,42</sup> neglect this volume dependence. Since the correlation functions for a random alloy are

$$\bar{\Pi}_{k,m}(R) = (2x - 1)^k, \quad (3.5)$$

all but the  $k=0$  term vanish at  $x = \frac{1}{2}$ . Hence,  $J_0$  at  $x = \frac{1}{2}$  gives the energy of the random alloy at this composition:  $\Delta H(R, x = \frac{1}{2}) = J_0(V(x = \frac{1}{2}))$ . Since  $J_0$  is by far the largest of all interaction energies at  $x = \frac{1}{2}$ , the energy of the random alloy at  $x = \frac{1}{2}$  dominate the expansion of Eq. (2.9).

(ii) Three- and four-body terms are rather small for semiconductor alloys.

(iii) Regarding the pair interactions  $J_{2,m}$  between  $m$  neighbors, we find  $J_{2,1}$  (first-neighbor pair) to be dominant. Yet the *fourth*-neighbor interactions  $J_{2,4}$  are larger than the second- ( $J_{2,2}$ ) and third-neighbor ( $J_{2,3}$ ) pair interactions. This result is found to hold for all eight semiconductor systems, and was previously noted<sup>32</sup> to hold in binary fcc transition-metal alloys. Figure 1 shows that  $J_{2,4}$  indeed encompasses the most direct path between non-first-neighbor atoms. This nonmonotonicity of  $J_{2,m}$  with  $m$ ,

$$|J_{2,1}| > |J_{2,4}| > |J_{2,2}| \simeq |J_{2,3}|, \quad (3.6)$$

serves as a warning against simple truncation of the energy expansion (2.2) on the basis of an hierarchy in  $m$ . Note (Fig. 1) that while  $J_{2,1}$  passes through a single  $C$  site, and  $J_{2,2}, J_{2,3}, J_{2,4}$  all pass through two  $C$  sites, further-neighbor interactions pass through *more* than two  $C$  sites and are hence considerably smaller.

### C. Formation and mixing enthalpies

Figures 4 and 5 show the reduced mixing enthalpy ("interaction parameter")

$$\hat{\Omega}(x, T) = \Delta H(x, T) / x(1-x) \quad (3.7)$$

for the disordered alloy at two temperatures (solid lines), and the analogous quantity (reduced formation enthalpy) for the ordered compounds  $s$  at  $T = 0$  K,

$$\hat{\Omega}_s(X_s, T = 0 \text{ K}) = \Delta E(s, V_s) / X_s(1-X_s), \quad (3.8)$$

depicted as solid diamonds. Table VI gives our calculated  $\hat{\Omega}(x, T)$  at  $x = 0, \frac{1}{2}$ , and 1 at  $T = 800$  K. In Ref. 20 we calculated  $\Delta H(x = \frac{1}{2}, T = 300 \text{ K})$  for GaAsSb using the same approach as here, but the fourth-neighbor pair interaction  $J_{2,4}$  was not included. This gave  $\Delta H(x = \frac{1}{2}, T = 300 \text{ K}) = 103 \text{ meV/four-atoms}$ , or  $\hat{\Omega}(x = \frac{1}{2}) = 4.75 \text{ kcal/mol}$ , instead of  $\Delta H(x = \frac{1}{2}, T = 800 \text{ K}) = 86 \text{ meV/four-atoms}$ , or  $\hat{\Omega}(x = \frac{1}{2}) = 3.96 \text{ kcal/mol}$  given here in Table VI.

The basic features of our results in Figs. 4 and 5 are as follows.

(i) For *size-mismatched* alloys, the (201)-type structures such as chalcopyrite have lower enthalpy than the disordered alloy. We will see in Sec. V that this will lead to *metastable long-range ordering of size-mismatched semiconductor alloys*, as indeed seen in liquid-phase-epitaxy growth of<sup>60</sup>  $\text{In}_{1-x}\text{Ga}_x\text{As}$  and in vapor growth of<sup>61-63</sup>  $\text{GaSb}_{1-x}\text{As}_x$ .

(ii) For *size-matched* alloys, the disordered alloy has a *lower* enthalpy than any of the studied simple ordered structures; hence *no thermodynamically mandated ordering is expected in size-matched semiconductor alloys*. The CuAu-I-like ordering seen by Kuan *et al.*<sup>64</sup> in  $\text{Al}_{1-x}\text{Ga}_x\text{As}$  is likely to be surface induced.

(iii) The CuPt phase, recently observed in epitaxial growth of size-mismatched semiconductor alloys,<sup>65-78</sup> is characterized by a considerably higher enthalpy than the disordered alloy; hence *bulk effects produce neither stable nor metastable CuPt ordering in size-mismatched semiconductor alloys*.

(iv)  $\hat{\Omega}(x, T)$  has a significant composition dependence, neglected by most previous phenomenological models.<sup>79-87</sup> Note that when  $B$  is the smallest of the two atoms in  $A_{1-x}B_x$ , we find that  $\hat{\Omega}(x=0) < \hat{\Omega}(x=1)$ . This reflects the fact that it requires more energy to incorporate a large atom  $A$  in a small host crystal  $B$  (i.e.,  $x \rightarrow 1$ ) than to incorporate a smaller atom  $B$  in a large

TABLE VI. Calculated miscibility-gap temperatures  $T_{\text{MG}}$ , composition  $x_{\text{MG}} = X(T_{\text{MG}})$ , interaction parameters  $\hat{\Omega}(x)$  of Eq. (3.7) at  $T = 800$  K, and spinodal ordering temperatures for a number of long-range-ordered phases (defined in Fig. 2 and Table XI).

	$T_{\text{MG}}$ (K)	$x_{\text{MG}}$	Interaction parameters (kcal/mol)			Ordering temperatures (K)			
			$\hat{\Omega}(0)$	$\hat{\Omega}(\frac{1}{2})$	$\hat{\Omega}(1)$	$T_{\text{CH}}$	$T_{\text{C1}}$	$T_{\text{C2}}$	$T_{\text{F1}}$
$\text{Al}_{1-x}\text{Ga}_x\text{As}$	64	0.49	0.30	0.30	0.30	0	0	0	0
$\text{GaAs}_{1-x}\text{P}_x$	277	0.603	0.53	0.86	1.07	75	91	67	80
$\text{In}_{1-x}\text{Ga}_x\text{P}$	961	0.676	2.92	3.07	4.60	463	305	215	450
$\text{GaSb}_{1-x}\text{As}_x$	1080	0.595	3.78	3.96	4.51	285	170	139	
$\text{In}_{1-x}\text{Ga}_x\text{As}$	630	0.770	2.68	2.35	3.56	320	167	136	80
$\text{Cd}_{1-x}\text{Hg}_x\text{Te}$	84	0.40	0.45	0.38	0.31	0	0	0	0
$\text{Hg}_{1-x}\text{Zn}_x\text{Te}$	455	0.560	2.13	1.88	2.15	256	135	87	200
$\text{Cd}_{1-x}\text{Zn}_x\text{Te}$	605	0.623	2.24	2.29	2.87	270	158	117	205

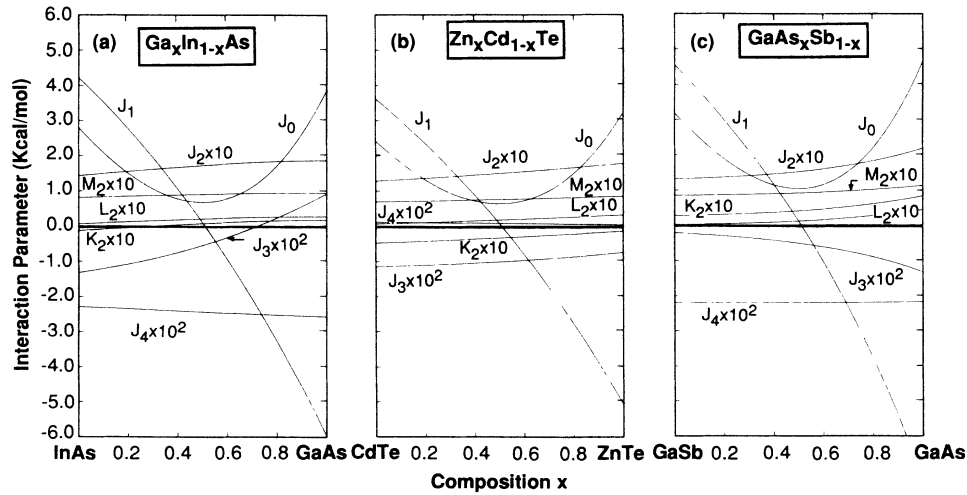


FIG. 3. Volume-dependent interaction energies  $J_{k,m}(V)$  for three semiconductor alloys; see Eq. (2.6). Here,  $J_{2,1} \equiv J_2$ ,  $J_{2,2} \equiv K_2$ ,  $J_{2,3} \equiv L_2$ , and  $J_{2,4} \equiv M_2$  are pair interactions from first, second, third, and fourth fcc neighbors.  $J_3$  and  $J_4$  are three- and four-body nearest-neighbor interactions, respectively.

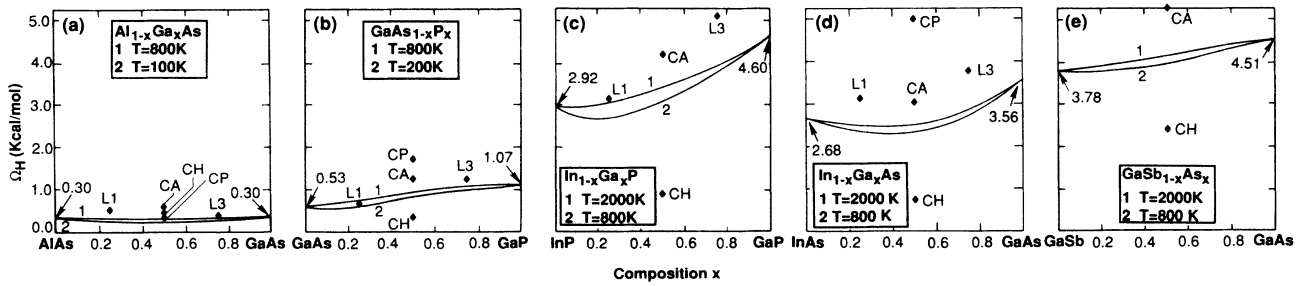


FIG. 4. Enthalpy interaction parameters  $\hat{\Omega}(x, T)$  [Eq. (3.7)] of the disordered alloys at two temperatures (solid lines), and the normalized formation enthalpies of ordered intersemiconductor compounds [Eq. (3.8), denoted by diamond-shaped symbols] for the III-V systems (a)  $\text{Al}_{1-x}\text{Ga}_x\text{As}$ , (b)  $\text{GaAs}_{1-x}\text{P}_x$ , (c)  $\text{In}_{1-x}\text{Ga}_x\text{P}$ , (d)  $\text{In}_{1-x}\text{Ga}_x\text{As}$ , and (e)  $\text{GaSb}_{1-x}\text{As}_x$ .

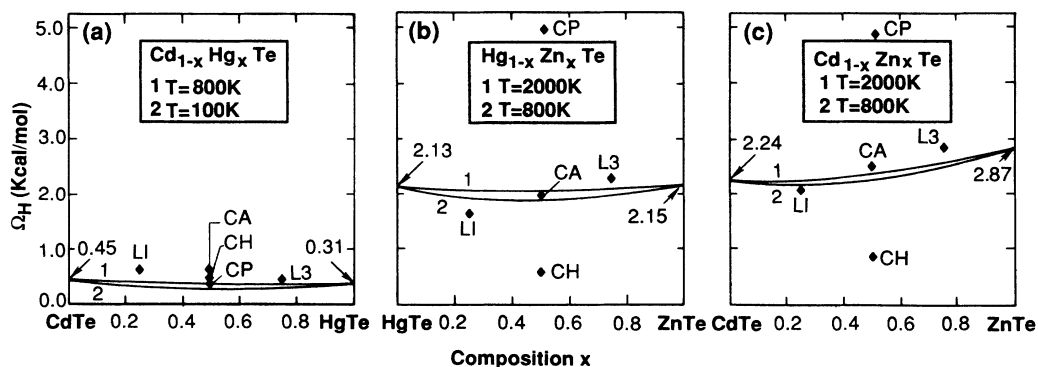


FIG. 5. Like Fig. 4 (see caption), but for the II-VI alloys (a)  $\text{Cd}_{1-x}\text{Hg}_x\text{Te}$ , (b)  $\text{Hg}_{1-x}\text{Zn}_x\text{Te}$ , and (c)  $\text{Cd}_{1-x}\text{Zn}_x\text{Te}$ .

host crystal  $A$  (i.e.,  $x \rightarrow 0$ ).

(v) Unlike the situation in metallic alloys,<sup>39</sup> no direct calorimetric measurements exist for  $\Delta H(x, T)$  in semiconductor alloys. Currently available values<sup>79–87</sup> were obtained by fitting the observed liquidus and solidus lines to simple thermodynamic models whose adjustable parameters include  $\hat{\Omega}$ . This procedure can lead to substantial uncertainties, depending on the type of model used and the number of parameters varied simultaneously, e.g., for  $\text{GaAs}_{1-x}\text{P}_x$  Brebrick and Panlener<sup>88</sup> find that  $\hat{\Omega} = -1.72$  or  $+2.06$  kcal/mol produce similar fits in strictly regular-solution models. Table VII compares our predicted values of  $\hat{\Omega}(x = \frac{1}{2}, T = 800 \text{ K})$  to the experimentally available data.<sup>79–87</sup> The results are also compared to the fit of Stringfellow<sup>89</sup> to his “delta-lattice-parameter” (DLP) model, those obtained by Martins and Zunger<sup>90</sup> from an elastic model, and to the empirical tight-binding perturbation model of Sher *et al.*<sup>91</sup> Our present first-principles results seem to agree with the available data, given the great uncertainty in the latter. However, better experimental precision will be needed to further assess the theoretical model. Despite the uncertainties, our parameter-free calculation does reproduce the global trends evident in the data, e.g., the rapid increase of  $\hat{\Omega}$  with the relative size mismatch  $|a_A - a_B|/|a_A + a_B|$  and its decrease with ionicity for a fixed size mismatch (e.g.,  $\text{Cd}_{1-x}\text{Zn}_x\text{Te}$  and  $\text{In}_{1-x}\text{Ga}_x\text{As}$  have a similar size mismatch, yet the former, more ionic, compound has a smaller  $\hat{\Omega}$ ).

(vi) The reduced enthalpy  $\hat{\Omega}(x, T)$  of disordered semiconductor alloys is temperature dependent, although this was neglected in simple phenomenological parametrizations of semiconductor-alloy phase diagrams.<sup>69–86</sup> Our calculated temperature dependence of  $\Delta H(x = \frac{1}{2}, T)$  is depicted in Figs. 6 and 7. Interestingly, as the temperature is lowered,  $\Delta H(x, T)$  becomes *less* positive. This reflects spatial correlations in the alloys which we discuss next.

#### D. Spatial correlations in the disordered phase

The calculated weights  $P_n(x, T)$  of Eq. (2.16) reflect the short-range order in the alloy as they measure the probability of finding cluster  $A_{4-n}B_n$  at  $(x, T)$ . In the simple case of a perfectly random ( $R$ ) alloy, the probability is given by

$$P_n^{(R)}(x) = \binom{4}{n} x^n (1-x)^{4-n}. \quad (3.9)$$

In Figs. 8 and 9 we depict the *excess* probability of the actual alloy relative to a random alloy at the same composition,

$$\Delta P_n(x, T) = P_n(x, T) - P_n^{(R)}(x). \quad (3.10)$$

It vanishes as  $T \rightarrow \infty$  when the alloy becomes perfectly random. Despite the fact that *both* size-matched and size-mismatched alloys have  $\Delta H(x, T) > 0$  and  $\Delta H_s > 0$ , and would hence appear to exhibit repulsive interactions, we find the following.

(i) For *size-matched* alloys,  $\Delta P_n(x, T)$  exhibits *enhancement* of the  $A_4$  (i.e.,  $n=0$ ) and  $B_4$  (i.e.,  $n=4$ ) clusters over what random statistics would grant (“clustering”), while the mixed  $AB_3$ ,  $A_2B_2$ , and  $A_3B$  clusters are generally *deficient* relative to the random alloy.

(ii) For *size-mismatched* alloys the opposite is true: the  $A_4$  and  $B_4$  clusters are *deficient*, while the mixed clusters are generally in *excess* (“anticlustering”). Clearly,  $\Delta H$  itself does not explain clustering versus anticlustering. This will be explained in Sec. IV B.

#### E. Phase diagrams

##### 1. Disordered phases

Figures 10 and 11 depict the calculated phase diagrams of the eight alloy systems in the high-temperature range where disordered alloys exist. The calculations show the binodal (“miscibility”) line as well as the spinodal. The

TABLE VII. Comparison of calculated interaction parameters (in kcal/mol) at  $T=800 \text{ K}$  [Eq. (3.7)] with values deduced from experiment (“model-dependent fits”) and with various calculations. These include the “delta-lattice-parameter” (DLP) model and the tight-binding (TB) perturbation model.

System	$\hat{\Omega}(\frac{1}{2})$ (present)	Model-dependent fits to data	DLP model <sup>l</sup>	Elastic model <sup>k</sup>	TB perturb. <sup>l</sup>
$\text{Al}_{1-x}\text{Ga}_x\text{As}$	0.30	0.0, <sup>a,b</sup> $-0.01^c$	0.00	0.0	$-0.07$
$\text{GaAs}_{1-x}\text{P}_x$	0.91	0.368, <sup>d</sup> 0.4, <sup>b</sup> 1.258, <sup>c</sup> 1.0 <sup>e</sup>	0.985	1.15	0.94
$\text{In}_{1-x}\text{Ga}_x\text{P}$	3.07	3.40, <sup>f</sup> 3.5, <sup>b</sup> 3.575, <sup>c</sup> 3.25 <sup>g</sup>	3.63	4.56	2.54
$\text{GaSb}_{1-x}\text{As}_x$	3.96	4.00, <sup>f</sup> 4.5, <sup>b</sup> 4.27 <sup>c</sup>	3.36	4.58	3.67
$\text{In}_{1-x}\text{Ga}_x\text{As}$	2.35	2.0, <sup>f</sup> 3.0, <sup>b</sup> 2.51, <sup>c</sup> 1.65 <sup>g</sup>	2.815	2.49	1.60
$\text{Cd}_{1-x}\text{Hg}_x\text{Te}$	0.38	1.40, <sup>h</sup> 0.72 <sup>i</sup>	0.00	0.00	$-0.07$
$\text{Hg}_{1-x}\text{Zn}_x\text{Te}$	1.88	3.0 <sup>h</sup>	1.81	1.91	1.50
$\text{Cd}_{1-x}\text{Zn}_x\text{Te}$	2.29	1.34 <sup>h</sup>	1.97	2.12	1.24

<sup>a</sup>Reference 79.

<sup>b</sup>Reference 80.

<sup>c</sup>Reference 81.

<sup>d</sup>Reference 82.

<sup>e</sup>Reference 83.

<sup>f</sup>Reference 84.

<sup>g</sup>Reference 85.

<sup>h</sup>Reference 86.

<sup>i</sup>Reference 87.

<sup>j</sup>Reference 89.

<sup>k</sup>Reference 90.

<sup>l</sup>Reference 91.

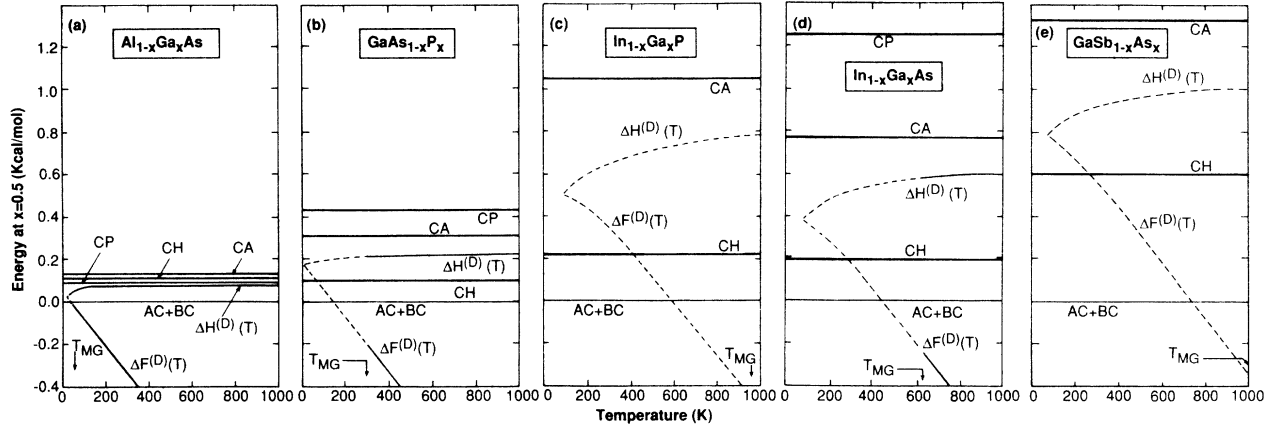


FIG. 6. Temperature dependence of the mixing enthalpy  $\Delta H^{(D)}(x = \frac{1}{2}, T)$  and free energy  $\Delta F^{(D)}(x = \frac{1}{2}, T)$  of the homogeneous disordered ( $D$ ) alloys and ordered compounds CH (chalcopyrite), CP (CuPt) and CA (CuAu). The arrows denote the miscibility-gap temperature where  $d^2\Delta F/dx^2$  changes sign. Dashed lines denote unstable regions. This figure gives results for the III-V alloys (a)  $\text{Al}_{1-x}\text{Ga}_x\text{As}$ , (b)  $\text{GaAs}_{1-x}\text{P}_x$ , (c)  $\text{In}_{1-x}\text{Ga}_x\text{P}$ , (d)  $\text{In}_{1-x}\text{Ga}_x\text{As}$ , and (e)  $\text{GaSb}_{1-x}\text{As}_x$ .

binodal is the line in the  $(x, T)$  plane where the  $A$ - and  $B$ -rich disordered phases have equal chemical potentials  $\mu$ . The spinodal line describes the limit of metastability of the disordered phase when  $d^2F/dx^2 = d\mu/dx = 0$ ,  $F$  being the free energy.

In all cases we find that the thermodynamically stable ground state corresponds to phase separation. The phase diagrams are generally asymmetric with respect to  $x = \frac{1}{2}$ . Table VI gives the calculated maximum miscibility-gap temperature  $T_{\text{MG}}$  and the composition  $x_{\text{MG}}$  where it occurs.

Experimental data on the solid-state part of semiconductor-alloy phase diagrams are fragmentary: While detailed data exist on the high-temperature liquidus and solidus lines,<sup>92</sup> the low atomic-diffusion con-

stants at lower temperatures make such studies in solid semiconductors difficult. A notable exception is the recent data of Ishida *et al.*<sup>93</sup> for  $\text{GaSb}_{1-x}\text{As}_x$  shown in Fig. 10(e), exhibiting close agreement with the calculation. Less complete results for this system are given by Gratton and Woolley.<sup>94</sup> Bublik *et al.*<sup>95</sup> have calculated the solid-solid phase diagram of a number of semiconductor alloys, finding for  $\text{GaAs}_{1-x}\text{P}_x$ ,  $\text{Al}_{1-x}\text{Ga}_x\text{As}$ ,  $\text{In}_{1-x}\text{Ga}_x\text{P}$ , and  $\text{In}_{1-x}\text{Ga}_x\text{As}$  miscibility-gap temperatures  $T_{\text{MG}}$  of 514, 400, 996, and 875 K, respectively. Using a simple-solution theory, Stringfellow<sup>96(a),96(b)</sup> calculated empirically the values 246, 0, 908, and 629 K [729 K in Ref. 96(c)], respectively, while for  $\text{GaSb}_{1-x}\text{As}_x$  he finds  $T_{\text{MG}} = 856$  K. In their semiempirical model,<sup>97</sup> Letardi *et al.*<sup>97(a)</sup> and Czyzyk *et al.*<sup>97(b)</sup> find a rather

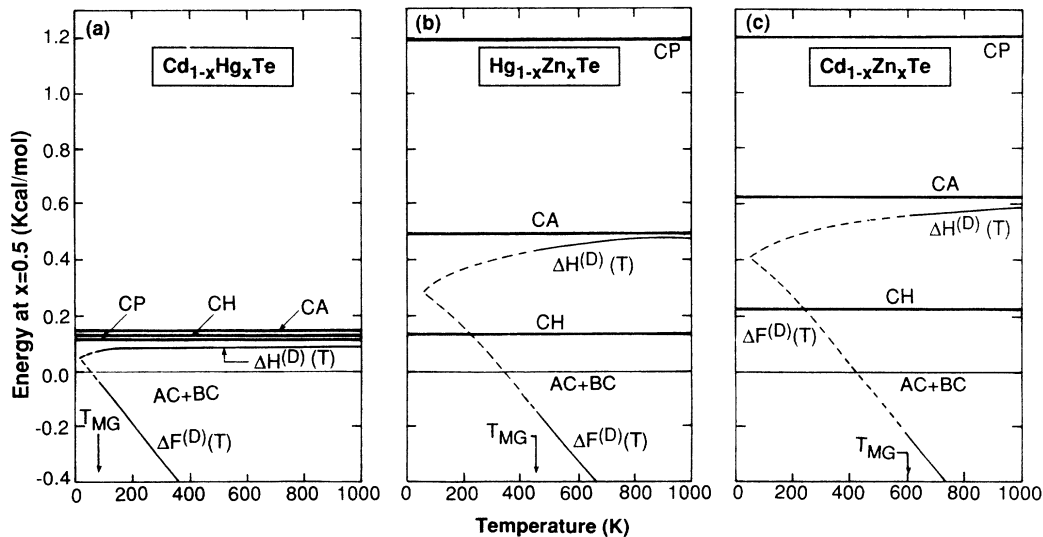


FIG. 7. Like Fig. 6 (see caption), but for the II-VI alloys (a)  $\text{Cd}_{1-x}\text{Hg}_x\text{Te}$ , (b)  $\text{Hg}_{1-x}\text{Zn}_x\text{Te}$ , and (c)  $\text{Cd}_{1-x}\text{Zn}_x\text{Te}$ .

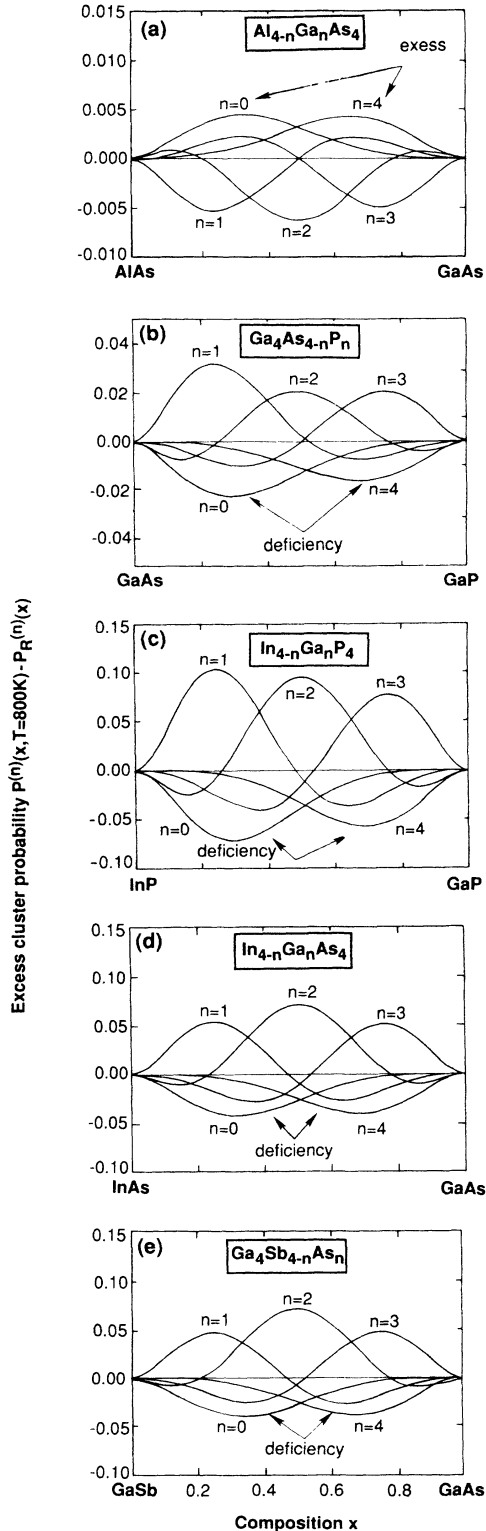


FIG. 8. Excess cluster probabilities  $P_n(x, T)$  at  $T=800$  K, with respect to the values obtained for a perfectly random ( $R$ ) alloy [Eq. (3.10)]. Observe the (small) clustering in the size-matched  $\text{Al}_{1-x}\text{Ga}_x\text{As}$  system and the (larger) anticlustering are found in the size-mismatched systems (all others). Results are given for the III-V systems whose clusters are denoted (a)  $\text{Al}_{4-n}\text{Ga}_n\text{As}_4$ , (b)  $\text{Ga}_4\text{As}_{4-n}\text{P}_n$ , (c)  $\text{In}_{4-n}\text{Ga}_n\text{P}_4$ , (d)  $\text{In}_{4-n}\text{Ga}_n\text{As}_4$ , and (e)  $\text{Ga}_4\text{Sb}_{4-n}\text{As}_n$  for  $0 \leq n \leq 4$ .

unusual phase diagram for  $\text{Cd}_{1-x}\text{Zn}_x\text{Te}$ ,  $\text{In}_{1-x}\text{Ga}_x\text{As}$ , and  $\text{In}_{1-x}\text{Ga}_x\text{P}$ , exhibiting a set of local minima and maxima in the binodal lines, which we do not find. Their  $T_{\text{MG}}$  values are 320, 483, and 620 K, respectively, while for  $\text{Al}_{1-x}\text{Ga}_x\text{As}$  they find  $T_{\text{MG}} \cong 360$  K.

## 2. Metastable ordered phases

The persistently lower formation enthalpy of the  $\text{ABC}_2$  chalcopyrite structure relative to the disordered phase in size-mismatched alloys (Figs. 4 and 5) suggests the possibility of metastable long-range ordering into this structure. We calculated the temperature limit of stability for this phase, according to

$$\frac{\partial^2 F}{\partial x^2} = 0. \quad (3.11)$$

The results are summarized in Table VI under “ordering temperature.” At thermodynamic equilibrium the system phase separates below  $T_{\text{MG}}$  into  $AC$ - plus  $BC$ -rich

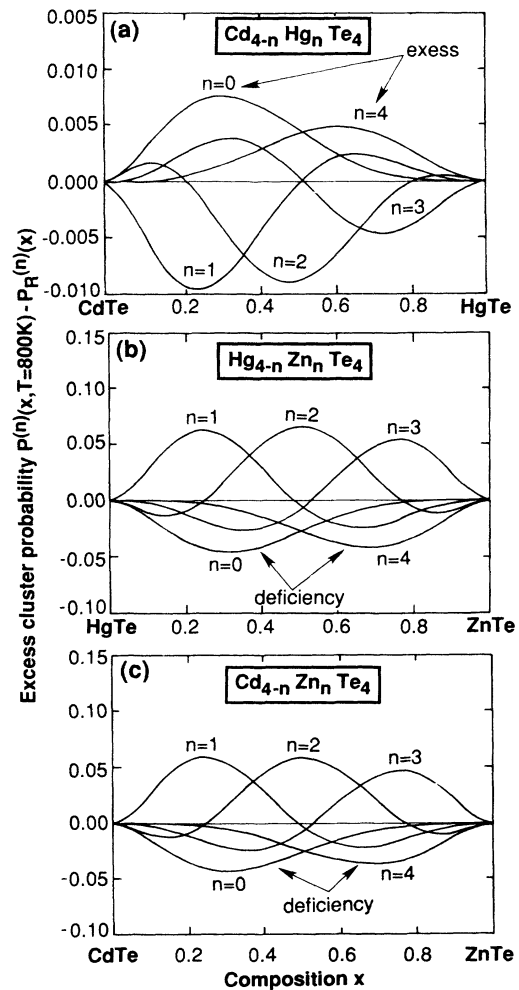


FIG. 9. Same as Fig. 8 (see caption), but for the II-VI alloys whose clusters are denoted (a)  $\text{Cd}_{4-n}\text{Hg}_n\text{Te}_4$ , (b)  $\text{Hg}_{4-n}\text{Zn}_n\text{Te}_4$ , and (c)  $\text{Cd}_{4-n}\text{Zn}_n\text{Te}_4$ .

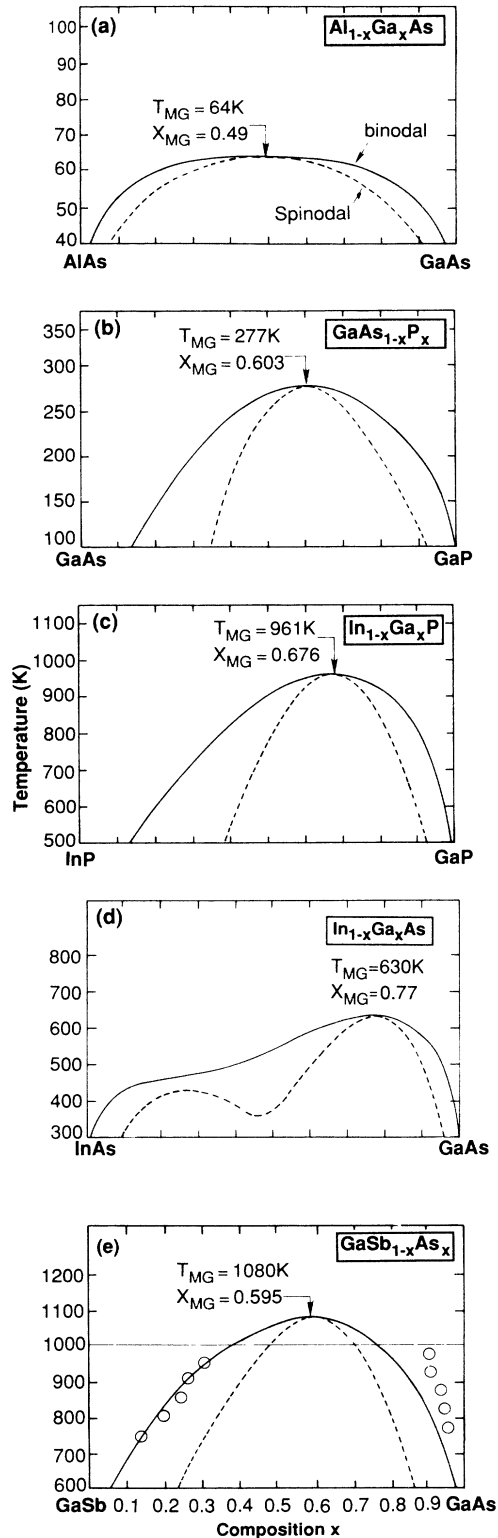


FIG. 10. Calculated phase diagrams for the III-V alloys (a)  $\text{Al}_{1-x}\text{Ga}_x\text{As}$ , (b)  $\text{GaAs}_{1-x}\text{P}_x$ , (c)  $\text{In}_{1-x}\text{Ga}_x\text{P}$ , (d)  $\text{In}_{1-x}\text{Ga}_x\text{As}$ , and (e)  $\text{GaSb}_{1-x}\text{As}_x$ . The solid (dashed) lines give the binodal (spinodal) lines. Low-temperature observed ordered phases are not shown (given in Tables VI, X, and XI). The arrows point to the maximum miscibility-gap (MG) temperatures and compositions. The circles in (e) are the recent experimental data of Ref. 93; the horizontal line represents the peritectic line.

mixtures, while above  $T_{\text{MG}}$  an homogeneous alloy persists. If, however, phase separation is kinetically inhibited, metastable long-range ordering will persist below  $T_c$  (Table VI). These structures are metastable in a very specific manner: they are *stabler* below  $T_c$  than the homogeneous disordered alloy, but *unstable* with respect to phase separation. Note that other ordered structures such as CuPt or CuAu-I are not metastable: they are *unstable* both with respect to disordering *and* phase separation. This result highlights the significance of interactions beyond first-nearest neighbors: retaining interactions only up to first neighbors ( $J_2$ ) leads to a degeneracy of the energies of the CuAu-I and chalcopyrite structures. Tables I (showing  $\Delta H_s$ ) and VI (showing  $T_c$ ) clearly demonstrate that this is not the case. A complete discussion of these ordered metastable phases is postponed to Sec. V, where a full search of ground state structures is discussed.

#### F. Alloy bond lengths

Equations (2.7) and (2.8) describe the proportion  $\xi_s(\sigma)$  that ordered clusters  $s$  occupy in an alloy of configuration  $\sigma$ . If each structure  $s$  has bond lengths  $R_{AC}(s, V(x))$  and  $R_{BC}(s, V(x))$  at composition  $x$ , the average alloy bond length can be described as

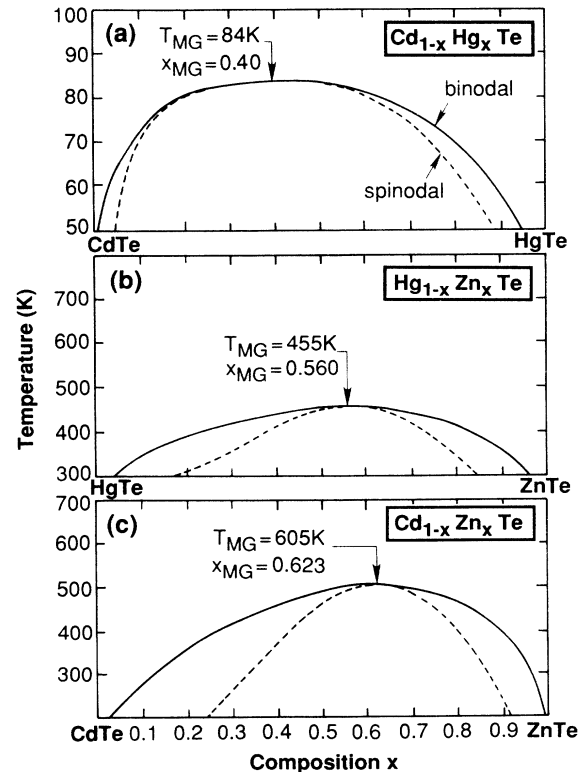


FIG. 11. Like Fig. 10 (see caption), but for the II-VI alloys (a)  $\text{Cd}_{1-x}\text{Hg}_x\text{Te}$ , (b)  $\text{Hg}_{1-x}\text{Zn}_x\text{Te}$ , and (c)  $\text{Cd}_{1-x}\text{Zn}_x\text{Te}$ .

$$R_{AC}(x) = \frac{1}{\omega(x)} \sum_s \xi_s(x) \omega_{AC}(s) R_{AC}(s, V(x)) \quad (3.12)$$

(and similarly for  $BC$ ), where  $\omega_{AC}(s)$  is the average number of  $AC$  bonds in structure  $s$ , and

$$\omega(x) = \sum_s \xi_s(x) \omega_{AC}(s). \quad (3.13)$$

In calculating  $\Delta E(s, V)$  for each structure, we also obtain  $R(s, V)$  (see Table I for the relaxation parameters determining the equilibrium bond lengths). Using these  $R(s, V)$  in Eq. (3.12), we calculate the composition dependence of the alloy bond lengths, depicted in Figs. 12 and 13. In this calculation a normalization factor  $v = a_{\text{eq}}^{\text{expt}} / a_{\text{eq}}^{\text{LDA}}$  has been used to scale the calculated LDA bond lengths for the pure binary compounds to agree with the experimental (expt) values. We show in Figs. 12 and 13 the “ideal” zinc-blende bond lengths  $R^0(A-C) = (\sqrt{3}/4)a_{AC}$  as dashed horizontal lines, and the linearly weighted average  $(1-x)R_{AC}^0 + xR_{BC}^0$  denoted  $\bar{R}(x)$ . Clearly, the equilibrium alloy bond lengths  $R_{AC}(x)$  and  $R_{BC}(x)$  deviate significantly from the average  $\bar{R}(x)$ , as noted first by Mikkelsen and Boyce<sup>40(a)</sup> and found in recent calculations.<sup>90,91</sup> These bond lengths also deviate somewhat from the “ideal” bond lengths  $R^0$  (by an amount highlighted in Figs. 12 and 13 by the shaded areas). These deviations freeze into the alloy a certain amount of strain energy. Indeed, alloys of pseudobinary semiconductors are “structurally frustrated,” in the sense that despite structural relaxations, the bond lengths and bond angles do not attain the “ideal,” strain-free values. The residual amount of frozen-in strain leads to positive excess enthalpies (Figs. 4 and 5).

### G. Effective equations of state

Equations (6.15) and (6.16) of Ref. 21 give the five effective equations of state  $\bar{\epsilon}_n(V)$  into which long-range

interactions have been folded. It is interesting to contrast these five effective equations of state with the results obtained without folding distant-neighbor interactions. To examine this we have fitted both equations to the expression of Murnaghan.<sup>58</sup> Tables IV and V give the parameters of the fit (denoted by an overtilde) and compare them to the corresponding parameters of the explicit equations of state. This comparison shows that the effective equilibrium volumes  $\bar{V}_n$  are unchanged for  $n=0$  and 4 (pure binary compounds), and are just slightly changed relative to  $V_n$  for  $n=1, 2$ , and 3. In contrast, the effective bulk moduli  $\bar{B}_n$  are dramatically reduced in the size-mismatched systems relative to  $B_n$ . This can be interpreted as follows. There are five possible local nearest-neighbor arrangements around a  $C$  atom in a fourfold-coordinated tetrahedral alloy, i.e.,  $A_4$ ,  $A_3B$ ,  $A_2B_2$ ,  $AB_3$ , and  $B_4$ . These five arrangements are geometrically identical to those encountered in the five (001)-type (Fig. 2) ordered compounds  $A_{4-n}B_nC_4$ , i.e., zinc-blende for  $n=0$  and 4,  $\text{CuAu-I}$  for  $n=2$ , and  $\text{Cu}_3\text{Au}$  for  $n=1$  and 3. The equilibrium molar volumes in these ordered compounds will be denoted  $V_n(X_n)$ , where  $X_n$  denotes the stoichiometry; the equilibrium molar volume of a disordered alloy will be denoted  $V(x)$ . While  $V_n(X_n)$  represents the equilibrium volume of cluster  $n$  embedded in an ordered structure, we will denote by  $V_n(x)$  the equilibrium volumes of such clusters in the disordered medium. One can take two extreme views of the relationship between the alloy values  $V_n(x)$  and those extracted from ordered compounds  $V_n(X_n)$ . (i) Assume that fixed atomic sizes can be associated with each type of atom; these radii (or molar volumes) can then be transferred with no change from one chemical environment to the other. This view, underlying Pauling’s concept of transferable atomic radii, implies

$$V_n(x) = V_n(X_n) \quad (\text{no relaxation}). \quad (3.14)$$

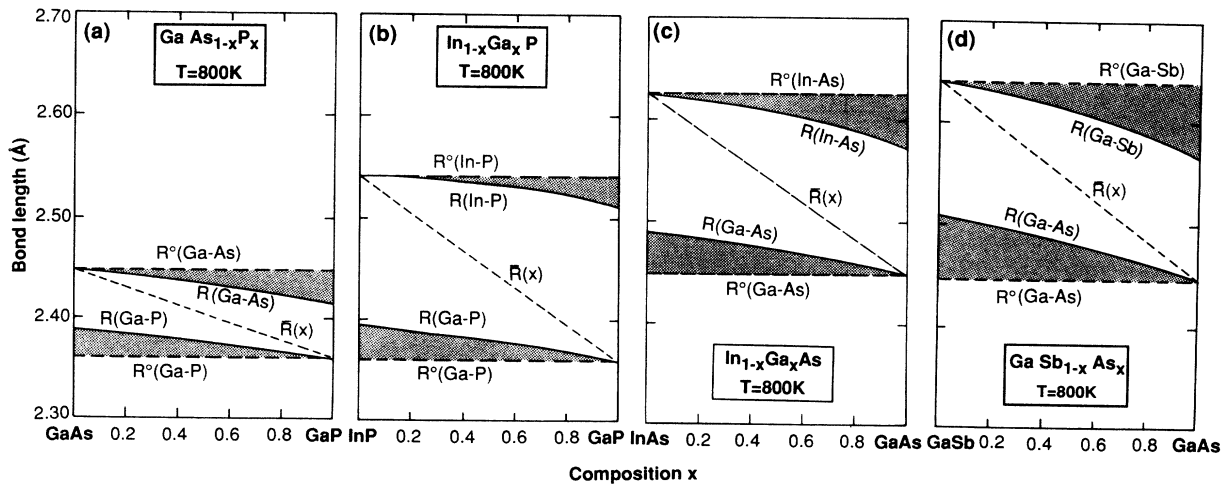


FIG. 12. Calculated equilibrium alloy bond lengths  $R(A-C)$  and  $R(B-C)$  at  $T=800$  K (solid lines), compared with the “ideal” zinc-blende values  $R^0(A-C)$  and  $R^0(B-C)$  (dashed horizontal lines). The composition-weighted average  $\bar{R}(x)$  is given for comparison. The shaded areas represent deviations of equilibrium alloy bond lengths from the “ideal” values. The strain, frozen-in due to such deviations leads to  $\Delta H > 0$ . Results are given for the size-matched III-V alloys (a)  $\text{GaAs}_{1-x}\text{P}_x$  (b)  $\text{In}_{1-x}\text{Ga}_x\text{P}$ , (c)  $\text{In}_{1-x}\text{Ga}_x\text{As}$ , and (d)  $\text{GaSb}_{1-x}\text{As}_x$ .

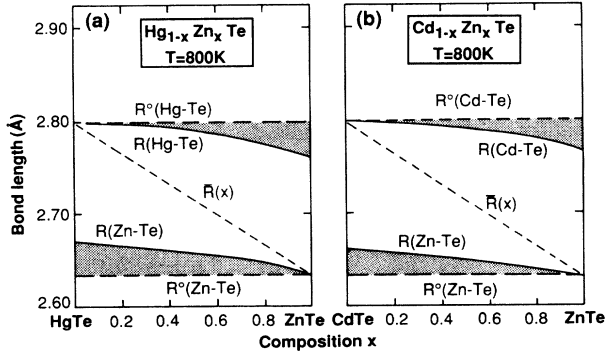


FIG. 13. Like Fig. 12 (see caption), but for the II-VI size-mismatched alloys (a)  $\text{Hg}_{1-x}\text{Zn}_x\text{Te}$  and (b)  $\text{Cd}_{1-x}\text{Zn}_x\text{Te}$ .

(ii) Assume alternatively that molar volumes are averaged in the alloy environment; hence,

$$V_n(x) = V(x) \quad (\text{full relaxation}) . \quad (3.15)$$

Both views are extreme cases of the Taylor-series expansion

$$V_n(x) = V_n(X_n) + K_n [V(x) - V_n(X_n)] + \dots . \quad (3.16)$$

Pauling's view [Eq. (3.14)] corresponds to no relaxation ( $K_n=0$ ), whereas the virtual-lattice model [Eq. (3.15)] corresponds to full relaxation ( $K_n=1$ ). Using Eq. (3.16), the effective excess energy of cluster  $n$  in the alloy is given for small volume changes by the harmonic expansion,

$$\begin{aligned} \Delta\bar{\epsilon}(n, V_n(x)) = & \Delta\tilde{H}_n + \frac{1}{2} \frac{B_n}{V_n} (1-K_n)^2 [V(x) - V_n(X_n)]^2 \\ & + \dots , \end{aligned} \quad (3.17)$$

where  $\Delta\tilde{H}_n$  is the relaxed effective energy at equilibrium.<sup>21</sup> Equation (3.17) can be mapped into an effective excess energy

$$\Delta\bar{\epsilon}(n, V_n(x)) = \Delta\tilde{H}_n + \frac{1}{2} \frac{\tilde{B}}{\tilde{V}_n} [V(x) - V_n(X_n)]^2 + \dots , \quad (3.18)$$

where

$$(1-K_n)^2 \equiv \frac{\tilde{B}_n}{B_n} \frac{V_n}{\tilde{V}_n} . \quad (3.19)$$

Our calculations, which include relaxation of all clusters, can be used to obtain the relaxation constants  $K_n$  from Eq. (3.19) and Tables IV and V. For  $n=2$ , for example, this gives

$$\begin{aligned} K_2(\text{GaAs}_{1-x}\text{P}_x) &= 0.132 , \\ K_2(\text{GaSb}_{1-x}\text{As}_x) &= 0.168 , \\ K_2(\text{In}_{1-x}\text{Ga}_x\text{P}) &= 0.157 , \\ K_2(\text{Hg}_{1-x}\text{Zn}_x\text{Te}) &= 0.198 , \\ K_2(\text{In}_{1-x}\text{Ga}_x\text{As}) &= 0.165 , \\ K_2(\text{Cd}_{1-x}\text{Zn}_x\text{Te}) &= 0.141 . \end{aligned} \quad (3.20)$$

The fluctuations of  $K_n$  about  $n=2$  are small. This demonstrates that the "softening" of the effective bulk moduli evident in Tables IV and V can be thought of as a relaxation effect associated with interactions outside the nearest-neighbor environment, and that this effective relaxation (13–20%) is considerably closer to Pauling's limit [Eq. (3.14)] than to the virtual-lattice limit [Eq. (3.15)].

#### IV. ANALYSIS OF TRENDS

This section analyzes the global trends underlying our results (Sec. III) in terms of a simple model in which the volume-dependent interaction energies  $\{J_f(V)\}$  are transformed into volume-independent energies  $\{v_f\}$  plus a global volume-dependent term.

##### A. Summary of regularities

Our foregoing discussion demonstrated a number of global features of semiconductor phase diagrams which we will now analyze. The salient trends are the following.

(i)  $\Delta H(x, T)$  is positive for all isovalent semiconductor alloys studied. It is about an order of magnitude larger in size-mismatched relative to size-matched alloys.

(ii) Despite this "universality," size-matched alloys show clustering, whereas size-mismatched alloys exhibit anticlustering.

(iii) Size-matched alloys do not exhibit any long-range-ordered phases, whereas size-mismatched alloys are predicted to exhibit universally a number of (201)-ordered phases at low temperatures.

(iv) There are obvious regularities in miscibility-gap temperatures  $T_{\text{MG}}$  and mixing enthalpies, both increasing with the relative size mismatch  $|a_A - a_B|^2 / |a_A + a_B|$ .

In what follows we present a simple model that analyzes these trends.

##### B. The $\epsilon$ -G approach

We found for semiconductor alloys<sup>21</sup> that while the equilibrium volume  $V(x)$ , the bulk modulus  $B(x)$ , and the latter's pressure derivative  $B'(x)$  all depend on composition, at a fixed composition these quantities are rather insensitive to the specific "state of order" (e.g., chalcopyrite versus CuPt versus CuAu-I for  $x = \frac{1}{2}$ ). A similar observation was made in Ref. 98 for transition-metal alloys. This opens the way to a simplification of the expansion of Eq. (2.1) which isolates explicitly volume-

dependent from volume-independent terms and is useful in analyzing chemical trends.

In Ref. 98 it was proved that if the equilibrium volume of the alloy at composition  $x$  does not depend on the state of order, the equation of state of configuration  $\sigma$  separates rigorously at the equilibrium volume  $V_{\text{eq}} = V(x)$  into the "spin-flip" or "substitutional" energies  $\varepsilon$  which depend on the state of order  $\sigma$ , but not on the volume, and the "elastic" energy  $G(V(x))$  which is volume dependent, but otherwise order independent. That is,

$$\Delta U(\sigma, V(x)) = \varepsilon(\sigma) + G(x). \quad (4.1)$$

Here we will generalize this "ε-G approach" to Eq. (2.1) with an arbitrary (but finite) number of interaction energies.

Assume that the equilibrium volume  $V(x)$ , the bulk modulus  $B(x)$ , and the latter's pressure derivative  $B'(x)$  are known as a function of  $x$  (and, hence, also at the stoichiometric composition  $x = X_s$ ). Specializing Eq. (4.1) to stoichiometric periodic structures  $\{s\}$  with arbitrary volume  $V$  gives the equation of state<sup>98</sup>

$$\Delta U(s, V) = \varepsilon^{(s)} + g(X_s, V), \quad (4.2)$$

where, as shown in Ref. 98,  $g(X_s, V)$  has the general form

$$\left. \frac{d^2 \Delta U(s, V)}{dV^2} \right|_{V=V_s} = Z[X(V)] \left. \left[ \frac{dX}{dV} \right]^2 \right|_{V=V_s} + [X(V) - X_s] \left. \left[ Z \frac{d^2 X}{dV^2} + \frac{dZ}{dX} \left[ \frac{dX}{dV} \right]^2 \right] \right|_{V=V_s} = \frac{B_s}{V_s} \quad (4.6)$$

at the equilibrium volume  $V_s$ . Thus,

$$Z(X_s) = \frac{B_s}{V_s} \left. \left[ \frac{dV}{dX} \right]^2 \right|_{V=V_s}. \quad (4.7)$$

(iv) Requiring the same pressure derivative  $B'_s$  sets the condition

$$\left. \frac{d^3 \Delta U}{dV^3} \right|_{V=V_s} = 3Z(X_s) \left. \frac{dX}{dV} \right|_{V=V_s} \left. \frac{d^2 X}{dV^2} \right|_{V=V_s} + 2Z'_s \left. \left[ \frac{dX}{dV} \right] \right|_{V=V_s}^2 = -\frac{B_s}{V_s^2} (B'_s + 1), \quad (4.8)$$

where  $Z'_s$  denotes the derivative of  $Z(x)$  with respect to  $x$  at  $x = X_s$ .

Had we known  $V(x)$ ,  $B(x)$ , and  $B'(x)$  for a continuous range of compositions, we could have calculated  $Z(x)$  so that it satisfies Eqs. (4.4)–(4.8) at all  $x$ 's. In practical applications we often know these quantities only on a discrete "grid" of compositions  $\{X_s\}$ . We will hence apply the conditions (4.4)–(4.8) to such a discrete set  $\{X_s\}$ . These conditions are then satisfied by selecting  $Z(x)$  as an interpolating polynomial which assumes the values  $Z(X_s)$  at the composition  $X_s$  [Eq. (4.7)] and has compositional derivatives  $Z'_s$  which satisfy Eq. (4.8). Dealing, for example, with five compositions  $X_s = 0, \frac{1}{4}, \frac{1}{2}, \frac{3}{4},$  and 1, the minimal polynomial passing through the five points  $Z(X_s)$  with given slopes  $Z'(X_s)$  is of the ninth degree. Its general form is

$$g(X_s, V) = (1 - X_s) \int_0^{X(V)} y Z(y) dy + X_s \int_{X(V)}^1 (1 - y) Z(y) dy. \quad (4.3)$$

For a carefully chosen function  $Z(y)$ , the equation of state  $\Delta U(s, V)$  of Eq. (4.2) can be made to have the same (given) physical parameters  $\Delta H_s$ ,  $V_s$ ,  $B_s$ , and  $B'_s$  as the true equation of state  $\Delta E(s, V)$  of structure  $s$ . This establishes the following conditions.

(i) Requiring  $\Delta U(s, V_s) = \Delta E(s, V_s)$  (i.e., the same formation enthalpy in both approaches) sets the condition that the substitution energy  $\varepsilon^{(s)}$  be obtained from the independently calculated  $\Delta H_s$  and  $G(X_s)$ ,

$$\Delta U(s, V_s) \equiv \Delta H_s = \varepsilon^{(s)} + G(X_s). \quad (4.4)$$

(ii) Requiring that the equilibrium volume  $V_s$  be the same in the two approaches in a set of compositions  $X_s$  [where  $V(X_s) = V_s$ ] gives the condition

$$\left. \frac{d \Delta U(s, V)}{dV} \right|_{V=V_s} = [X(V) - X_s] Z[X(V)] \left. \frac{dX}{dV} \right|_{V=V_s} = 0, \quad (4.5)$$

which is naturally satisfied at  $X(V_s) = X_s$ .

(iii) Requiring the same bulk moduli in the two approaches sets the condition

$$Z(x) = \sum_n \left[ Z_n + (x - X_n) \left[ Z'_n - \sum_{j(\neq n)} \frac{2Z_n}{X_n - X_j} \right] \right] \times \prod_{j(\neq n)} \frac{(x - X_j)^2}{(X_n - X_j)^2}, \quad (4.9)$$

where  $Z_n = Z(X_n)$ . With  $Z(x)$  defined as above,  $\Delta U(s, V)$  of Eq. (4.2) has all the required properties of  $\Delta E(s, V)$  on the grid of points  $\{X_s\}$ . A potential source of error is then the use of an interpolation between these points.

Because the function  $\Delta U(s, V)$  has the virtue that its volume-dependent term  $g(X, V)$  is linear in composition  $X_s$  [Eq. (4.3)], the configurational energy can be written as

$$\Delta U(\sigma, V) = G(x) + \sum_f D_f v_f \bar{\Pi}_f(\sigma), \quad (4.10a)$$

and the excess enthalpy for the alloy [ensemble average of Eq. (2.7)] can be written as a superposition of  $\Delta U(s, V)$  of Eq. (4.1) instead of  $\Delta E(s, V)$  as

$$\Delta \bar{H}(x, T) = \langle \Delta U(\sigma, V) \rangle = G(x) + \sum_s \langle \xi^{(s)}(x, T) \rangle \varepsilon^{(s)}, \quad (4.10b)$$

or

$$\Delta \bar{H}(x, T) = \langle \Delta U(\sigma, V) \rangle = G(x) + \sum_f D_f v_f \langle \bar{\Pi}_f \rangle, \quad (4.10c)$$

where  $v_f$  are *volume-independent* interactions energies given, in analogy with Eq. (2.6), by

$$v_f = \frac{1}{ND_f} \sum_s [\bar{\Pi}_f(s)]^{-1} \varepsilon^{(s)}. \quad (4.11)$$

The substitution energies  $\varepsilon^{(s)}$  are given by Eq. (4.4), while

$$G(x) = (1-x) \int_0^x y Z(y) dy + x \int_x^1 (1-y) Z(y) dy. \quad (4.12)$$

The “ $\varepsilon$ - $G$ ” form of the excess energy  $\Delta U(s, V)$  is evaluated as follows. (i) Using  $\{V_s, B_s, B'_s\}$  at the five compositions  $X_s = 0, \frac{1}{4}, \frac{1}{2}, \frac{3}{4},$  and 1, we evaluate  $Z(X_s)$  of Eq. (4.7) and  $Z(x)$  for all  $x$ 's from Eq. (4.9). (ii) Integration of Eq. (4.12) with this  $Z(x)$  provides the elastic energy function  $G(x)$ . (iii) Using the values of  $G(x)$  at  $x = X_s$  and the eight formation enthalpies  $\Delta H_s$ , we obtain from Eq. (4.4) the eight substitution energies  $\{\varepsilon^{(s)}\}$ . (iv) To obtain the volume-independent interaction energies  $\{v_f\}$  for the figures  $f$ , we use Eq. (4.11).

Since the equations of state  $\Delta U(s, V)$  reproduce the first three volume derivatives of  $\Delta E(s, V)$  and have the same minimum energy  $\Delta H_s$ , these two sets can be essentially used interchangeably. However, the  $\varepsilon$ - $G$  form has the added virtue in that it transparently separates energies associated with volume changes (“elastic” effects) from constant-volume energy changes (“chemically”).

### C. Testing the $\varepsilon$ - $G$ approach

To convince the reader that there is no significant loss of precision in using  $\Delta \bar{H}(x, T)$  of Eq. (4.10) (i.e., the volume-independent representation of  $v_f$  termed “model a” in Table VIII) instead of Eq. (2.1) [the volume-dependent representation of  $J_f(V)$ , termed “model b”], we compare the transition temperatures obtained from a CVM solution to both Hamiltonians. The results for  $\text{GaSb}_{1-x}\text{As}_x$  are presented in the first two columns of Table VIII and indicate only small deviations.

It is useful to present the results of the  $\varepsilon$ - $G$  approach in close form, i.e., represent the (numerically obtained) function  $G(x)$  by an analytical expression. This can be done, e.g., by using the form

$$G(x) \cong x(1-x)\Omega(x), \quad (4.13)$$

where  $\Omega(x)$  is a two-parameter linear function,

$$\Omega(x) = \alpha + \beta(x - \frac{1}{2}). \quad (4.14)$$

The parameters are determined by equating the areas of

TABLE VIII. Comparison of miscibility-gap temperatures ( $T_{\text{MG}}$ ) and composition  $x_{\text{MG}} = X(T_{\text{MG}})$ , as well as the order-disorder temperatures of various long-range-ordered phases as obtained by three model Hamiltonians for  $\text{GaSb}_{1-x}\text{As}_x$ : (a) Eq. (4.10a) using the volume-independent  $\{v_f\}$  representation plus the (numerically calculated) elastic energy  $G(x)$ , (b) Eq. (2.2) using the volume-dependent  $\{J_f(V)\}$  representation, and (c) like (a), but using an analytic fit [Eqs. (4.13)–(4.16)] to  $G(x)$ .

	Model a using $\{v_f\}$ [Eq. (4.10a)]	Model b using $\{J_f(V)\}$ [Eq. (2.2)]	Model c using $\{v_f\}$ + fitted $G(x)$
$T_{\text{MG}}$ (K)	1075	1080	1122
$x_{\text{MG}}$	0.656	0.595	0.692
$T_{\text{CH}}$ (K) <sup>a</sup>	287	285	285
$T_{\text{C1}}$ (K) <sup>a</sup>	153	170	153
$T_{\text{C2}}$ (K) <sup>a</sup>	165	139	163

<sup>a</sup>Phases CH, C1, and C2 are explained in Table XI.

the functions  $G(x)$  and  $(x - \frac{1}{2})G(x)$  on either side of Eq. (4.13), giving

$$\alpha = 3 \int_0^1 x(1-x)Z(x)dx, \quad (4.15)$$

$$\beta = 10 \int_0^1 x(1-x)(2x-1)Z(x)dx, \quad (4.16)$$

where  $Z(x)$  of Eq. (4.9) satisfies  $Z(x) = -d^2G(x)/dx^2$ . To test this analytical form of the  $\varepsilon$ - $G$  representation, we give in the third column of Table VIII (“model c”) the results obtained using the CVM solution to this form of the  $\varepsilon$ - $G$  approach (here,  $\alpha = 10.93153$  kcal/mol and  $\beta = 2.38501$  kcal/mol). The results show only a negligible loss of precision relative to the complete  $\varepsilon$ - $G$  solution (“model a”).

Table I gives the substitution energies  $\varepsilon^{(s)}$  for the semiconductors studied here; Table IX gives  $\{v_f\}$  for these alloy systems. It also includes a simpler, one-parameter fit of  $G(x) = \bar{\Omega}x(1-x)$ , which, while not as accurate as the two-parameter fit of Eqs. (4.13)–(4.16) (it yields  $T_{\text{MG}} = 956$  K,  $T_{\text{CH}} = 285$  K,  $T_{\text{C1}} = 147$  K,  $T_{\text{C2}} = 170$  K), it is more convenient. These define completely the Ising Hamiltonian in either of the three forms of Eqs. (4.10). It can be solved by any of the available techniques (e.g., MC, CVM), yielding practically the same results obtained in Sec. III using  $\{J_f(V)\}$ . Note that size-matched alloys have  $v_{2,1} < 0$  (ferromagnetic repulsion), while  $v_{2,3}$  and  $v_{2,4}$  are positive (antiferromagnetic attraction). In contrast, size-mismatched alloys exhibit positive (i.e., attractive)  $v_{2,1}$ ,  $v_{2,3}$ , and  $v_{2,4}$ . Figure 14 depicts for these alloys  $G(x = \frac{1}{2})$  and  $\varepsilon^{(s)}$  for the three ordered  $x = \frac{1}{2}$  structures, and that for the disordered alloy at  $T = 800$  K.

### D. Analysis of trends in the $\varepsilon$ - $G$ representation

The  $\varepsilon$ - $G$  representation of the mixing enthalpy of Eq. (4.10) is not only useful in quantitatively reproducing phase diagrams (Table VIII), but also makes a number of physical trends transparent.

(i) We find (Fig. 14) that the lattice-matched systems (AlAs-GaAs and CdTe-HgTe) have  $G \approx 0$  and  $\varepsilon^{(s)} > 0$ , whereas the lattice-mismatched systems have  $G > 0$  and

TABLE IX. Volume-independent interaction energies  $2v_{k,m}$  of the Ising model of Eq. (4.10a) (in meV) and the average elastic energy parameter  $\bar{\Omega}$  (in meV/four-atoms) corresponding to the  $G(x) = \bar{\Omega}x(1-x)$  approximation. Here,  $k$  denotes the number of sites interacting simultaneously;  $m$  is the neighbor separation.

Interaction energy	$D_f$	AlAs GaAs	GaP GaAs	GaP InP	GaSb GaAs	InAs GaAs	HgTe CdTe	HgTe ZnTe	CdTe ZnTe
$2v_{0,1}$	1	6.6047	-47.8160	-240.1940	-145.9788	-164.6280	7.8761	-161.8135	-129.4630
$2v_{1,1}$	1	-0.1518	3.5594	5.3439	-3.4977	-1.6352	-1.6046	-0.6551	1.9546
$2v_{2,1}$	6	-1.591	4.7822	23.9011	13.2334	15.5053	-1.5633	14.8303	13.1823
$2v_{3,1}$	8	0.0190	-0.4449	-0.6679	0.4372	0.2044	0.2006	0.0819	-0.2443
$2v_{4,1}$	2	0.0190	1.2138	0.3793	-1.8617	-1.6893	0.0650	-0.0144	0.1952
$2v_{2,2}$	3	0.1757	-0.8604	-1.3832	3.5176	0.6822	-0.1166	-3.1839	-2.9110
$2v_{2,3}$	12	0.0757	0.1568	2.4495	0.9876	2.0151	0.0427	3.0225	1.5586
$2v_{2,4}$	6	0.2443	2.899	11.7974	8.0036	8.1244	0.2020	7.6905	6.6681
$\bar{\Omega}$		0.0000	269.6946	1287.2400	948.5059	893.0924	1.9870	838.0564	739.1497

$\epsilon^{(s)} < 0$ . Hence, while  $\Delta H(x, T)$  and  $\Delta H_s$  are positive in both classes of systems, this is so for different reasons: unfavorable chemical interactions in the first case (where sublattice relaxation is small owing to  $R_{AC}^0 \cong R_{BC}^0$ ), and strong, repulsive elastic interactions in the second case. These different origins of  $\Delta H > 0$  have a number of immediate implications.

(ii) Both  $\Delta H(x = \frac{1}{2}, T)$  and  $\Delta H_s$  are about an order of magnitude smaller in lattice-matched systems than in lattice-mismatched systems since “stiff” bulk moduli and significant size differences combine to produce in the latter case larger elastic energies  $G(x)$  which overwhelm

the smaller chemical energies.

(iii) The relative population  $P^{(n)}(x, T)$  of clusters  $n$  at a fixed composition  $x$  is unaffected by  $G(x)$ , which is common to all clusters at the same  $x$ . Hence, systems with  $\epsilon^{(s)} > 0$  (AlAs-GaAs and CdTe-HgTe in Fig. 14) exhibit clustering (Figs. 8 and 9)—enhancement of the  $A_4$  and  $B_4$  clusters—whereas systems with  $\epsilon^{(s)} < 0$  exhibit “anti-clustering” (Figs. 8 and 9). This highlights the fact that knowledge of  $\Delta H$  alone is insufficient to judge such effects, and its decomposition into  $\epsilon$  and  $G$  is necessary.

(iv) An order-disorder transition at a fixed composition  $X_t$  occurs when the free energies of the ordered and disordered phases are equal. Since  $G(X_t)$  is common to both phases at  $X_t$ , it does not determine the transition temperature  $T_t$ —this is determined by the substitution energies alone. Hence, lattice-matched alloys having  $\epsilon^{(n)} > 0$  do not exhibit any (stable or metastable) simple ordered states, while lattice-mismatched alloys, having  $\epsilon^{(n)} < 0$ , can exhibit metastable long-range-ordered phases. Figure 14 shows that at  $x = \frac{1}{2}$  only the chalcopyrite phase has a substitution energy lower than that of the random alloy; hence, it alone will show up at this composition as a metastable ordered phase.

(v) The order of the formation enthalpies for the different structures given in Eqs. (3.1) and (3.2) reflects the order of the substitution energies (Fig. 14).

#### E. Comparison of Monte Carlo and CVM solutions to the Ising Hamiltonian

Another advantage of the representations (4.10) of the Ising Hamiltonian is its amenability to Monte Carlo simulations, which are considerably more difficult when  $J_f$  are functions of volume. To assess the validity of our folding method, whereby second-, third-, and fourth-neighbor pair interactions are renormalized into effective nearest-neighbor interactions  $\bar{J}(x, V)$ , we compare the CVM solution of this Ising Hamiltonian [Eq. (4.10a)], including folding, to a MC solution of the full (unfolded) Hamiltonian.

For simplicity we select in Eq. (4.10a)  $G(x) = \bar{\Omega}x(1-x)$  and remove the three- and four-body terms, i.e.,  $v_{3,1} = v_{4,1} = 0$ . We find  $\bar{\Omega}$  through Eq. (4.13) using  $\bar{\Omega} = \bar{\Omega}(x)$ . These simplifications lead to a phase diagram which is symmetric about  $x = \frac{1}{2}$ , and the two-phase

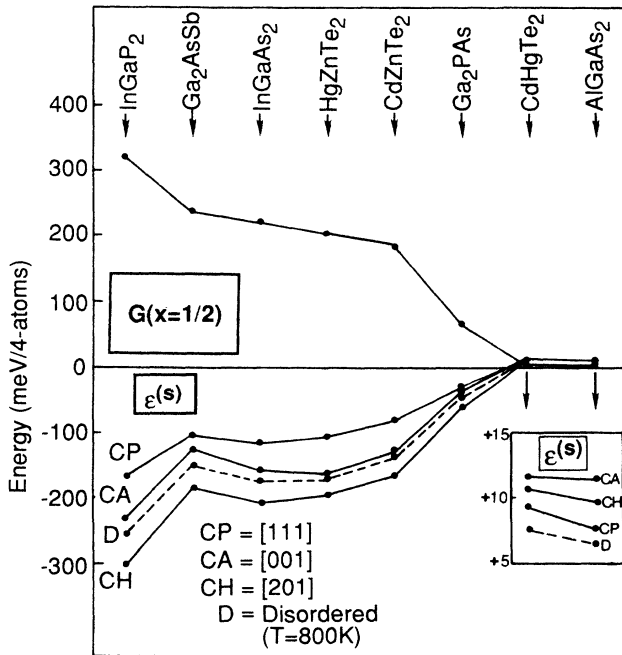


FIG. 14. Breakdown of the formation enthalpies of ordered 50%-50% intersemiconductor compounds CP (CuPt), CA (CuAu), and CH (chalcopyrite) into elastic  $G(x = \frac{1}{2})$  and substitutional  $\epsilon^{(s)}$  pieces [Eq. (4.4)]. For comparison, we also give the substitutional energy for the disordered 50%-50% alloy at  $T = 800$  K. Note that  $\epsilon^{(s)} > 0$  (inset) for the two size-matched alloys.

equilibrium occurs at the chemical potential  $\mu=0$ . Thus, the search for the phase-equilibrium lines in the  $(\mu, T)$  plane (a very time-consuming step in MC) is simplified. The parameters used, appropriate to  $\text{GaSb}_{1-x}\text{As}_x$ , are (in meV)

$$v_{2,1}=6.6167, \quad v_{2,2}=1.7588, \quad (4.17a)$$

$$v_{2,3}=0.4938, \quad v_{2,4}=4.0018,$$

$$v_{0,1} = - \sum_m D_{2,m} v_{2,m} = -74.913, \quad (4.17b)$$

and  $\bar{\Omega}=948.5059$  meV/four-atoms.

Note that the *volume-independent* Hamiltonian of Eqs. (4.10) satisfies the sum rules

$$v_{0,1} = - \sum_k \sum_m^{\text{even}} D_{k,m} v_{k,m}, \quad (4.18)$$

$$v_{1,1} = - \sum_k \sum_m^{\text{odd}} D_{k,m} v_{k,m}$$

evident in Table IX. These sum rules do not apply to the volume-dependent energies  $J_{k,m}(V)$ . Our  $v_{0,1}$  of Eq. (4.17a) differs from the value given in Table IX since in the former case  $v_{3,1}=v_{4,1}=0$ , and, hence, the sum rules yield a slightly different  $v_{0,1}$ .

Via use of Eq. (4.10c), the excess enthalpy of this spin- $\frac{1}{2}$  three-dimensional fourth-nearest-neighbor Ising Hamiltonian is

$$\begin{aligned} \Delta H(x) = & \bar{\Omega}x(1-x) + v_{0,1} + 6v_{2,1}\langle \bar{\Pi}_{2,1} \rangle + 3v_{2,2}\langle \bar{\Pi}_{2,2} \rangle \\ & + 12v_{2,3}\langle \bar{\Pi}_{2,3} \rangle + 6v_{2,4}\langle \bar{\Pi}_{2,4} \rangle, \end{aligned} \quad (4.19)$$

where  $v_{k,m}$  represents the  $m$ th-neighbor pair interaction. Although this simplified Hamiltonian is not designed to capture the full detail of the phase diagram in which the complete  $G(x)$  as well as three- and four-body terms are retained (Table VIII), its parallel solution via the MC method and the CVM with folding will serve to assess the validity of our folding method, in which

$$\langle \bar{\Pi}_{2,2} \rangle = \langle \bar{\Pi}_{2,3} \rangle = \langle \bar{\Pi}_{2,4} \rangle = \langle \bar{\Pi}_{1,1} \rangle^2. \quad (4.20)$$

The Monte Carlo runs were made using single-spin-flip kinetics.<sup>99</sup> We used a cell of  $12^3=1728$  fcc sites, with 100 flip attempts per site to reach steady state and 400 attempts per site to collect data. The acceptance ratio, which is defined as the fraction of successful flip attempts, was minimum at 700 K, when it attained a value of 19%, and increased fast as the temperature was raised.

The results are presented in Figs. 15 and 16. The binodal points of Fig. 15(a) were determined by starting from a random sample with  $x=0.99$ , letting it stabilize, and collecting data at  $\mu=0$ . Above 850 K and below  $T_{\text{MG}}$ , the spin-flip process led to a two-phase system and the sample oscillated between these two phases in equilibrium. Thus, it was impossible to determine accurately the equilibrium concentration of each phase. Although the oscillations of  $x$  are large, we observed that the probability of finding pairs  $AB$ , which is equal in the two phases, had small oscillations. Therefore we used this fact to find the critical temperature according to the construction of

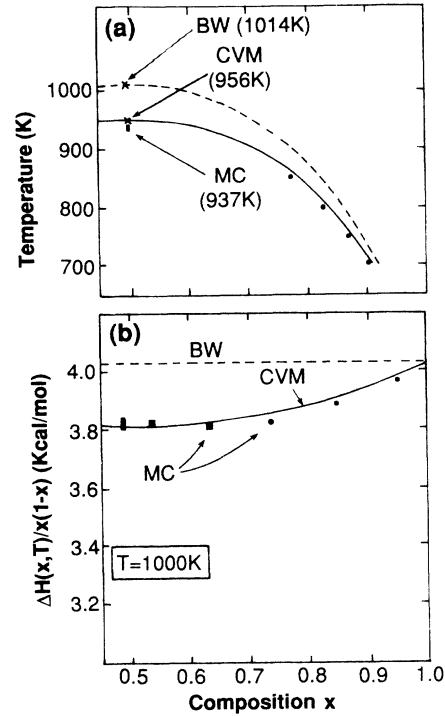


FIG. 15. (a) Phase diagram (binodal) for CVM with folded distant-neighbor interaction (solid line), Bragg-Williams method (BW, dashed line), and Monte Carlo method (MC, dots and bar). The Hamiltonian is given in Eqs. (4.17)–(4.19). (b) gives the normalized mixing enthalpies for these three models. The rectangles depicting Monte Carlo results have the size of the standard deviation in  $x$  and  $\Delta H/x(1-x)$ . The standard deviation is smaller than the sizes of the solid circles.

Fig. 16. Figure 15(b) presents the interaction parameter at 1000 K. In all cases, the dots, bars, or rectangles have size equal or greater than the standard deviation. We have also included for comparison results obtained by the mean-field Bragg-Williams (BW) approach<sup>100</sup> in which all correlations are neglected, and one has

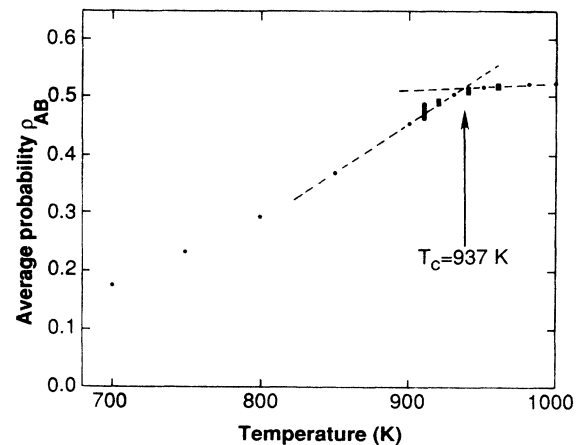


FIG. 16. Average nearest-neighbor ( $A-B$ ) pair probability in the Monte Carlo calculation (Fig. 15) as a function of temperature. The crossing point is used to determine the transition temperatures of Fig. 15.

$$\langle \bar{\Pi}_{2,m} \rangle_{\text{BW}} = (2x - 1)^2 \quad (4.21)$$

and

$$\Delta H_{\text{BW}}(x) = x(1-x)(\bar{\Omega} + 4v_{0,1}), \quad (4.22)$$

with

$$v_{0,1} = -6v_{2,1} - 3v_{2,2} - 12v_{2,3} - 6v_{2,4}. \quad (4.23)$$

Figure 15 shows an excellent agreement between the phase diagram [Fig. 15(a)] and mixing enthalpy [Fig. 15(b)] obtained from Monte Carlo and CVM solutions. We conclude that our tetrahedron CVM with folded distant pair interactions in no way worsens the good agreement between standard CVM and MC methods. Thus, the folding method opens the way to the inclusion in CVM of more realistic and complicated Hamiltonians.

## V. THE SEARCH FOR GROUND STATES

The use of the energy expansion in terms of multistate-interaction energies [Eqs. (2.1) or (4.10)] and the determination of the interaction energies permits us to capitalize on known results<sup>101,102</sup> from Ising-model studies on the allowable ground states supported by this Hamiltonian. The basic problem is to identify those structures which minimize the energy expression (4.10) at each composition  $x$ . The stability analysis is most simply made in the  $\epsilon$ - $G$  formalism, where the configuration  $\sigma$  has the energy given by Eq. (4.10a). We will refer to the second term of this equation as the “chemical” energy  $\Delta E_{\text{chem}}(\sigma)$ . To establish the stability conditions, we proceed in two steps.

(i) *Constant-composition (homogeneous equilibrium) search:* First, we compare structures with fixed composition  $x$ , and search for the lowest energy at each  $x$ . In this case the term  $G(x)$  is not considered because it is common to all structures at the same  $x$ ; this procedure is precisely what is done in usual studies of Ising models<sup>101,102</sup> with *fixed* interactions  $v_f$ , i.e., neglecting  $G(x)$ . The ground states for a fcc Ising Hamiltonian containing up to second-neighbor terms is well known;<sup>101</sup> these are partially known if the interactions are extended up to the fourth neighbor.<sup>102</sup> Since the correlation functions  $\bar{\Pi}_f(\sigma)$  determine the probability of the figures in configuration  $\sigma$ , and since the probabilities must be positive, the correlations  $\bar{\Pi}_f$  are limited to a configurational polyhedron in the space of  $\{\bar{\Pi}_f\}$ . Because the Hamiltonian is linear in the correlation functions, the vertices of the polyhedron represent states of order whose energies are extrema. For an arbitrary composition  $x$ , the minimum energy will be that of a linear combination of the energies of *two* vertices 1 and 2:

$$\Delta E(x) = \Delta E(\sigma_{\text{min}}) = G(x) + \xi_1 \epsilon^{(1)} + \xi_2 \epsilon^{(2)}, \quad (5.1)$$

where  $\xi_1$  and  $\xi_2$  satisfy

$$\xi_1 + \xi_2 = 1, \quad (5.2)$$

$$X_1 \xi_1 + X_2 \xi_2 = x, \quad (5.3)$$

or

$$\xi_1 = \frac{x - X_2}{X_1 - X_2}, \quad (5.4)$$

$$\xi_2 = \frac{x - X_1}{X_2 - X_1}, \quad (5.5)$$

$X_1$  and  $X_2$  being the composition at the vertices. Kanamari and Kakehashi<sup>102</sup> performed such a constant-composition ground-state study of the fcc Ising Hamiltonian with pair interactions extending to fourth neighbors. Their study is, however, only partially useful for our aim here, since they excluded three- and four-body interactions and limited the search for Hamiltonians where the nearest-neighbor interaction  $v_{2,1}$  dominates all other pair interactions. Our first-principles study shows (Fig. 3 and Table IX) that this promise is not satisfied in semiconductors where  $v_{2,4}$  is competitive with  $v_{2,1}$ . We have hence repeated and generalized Kanamari’s study to include three- and four-body terms and treat all  $v_{2,m}$  equally for all  $m$ ’s up to  $m=4$ . We limited, however, the search to unit cells containing up to 15  $A$  or  $B$  atoms (Kanamari included up to 16-atom structures). Despite this limitation, our study gives a reasonable description of the ground-state line and identifies the most important vertices of the not considered polyhedron. The ground-state structures [with  $G(x)=0$ ] found in the six lattice-mismatched alloys are given in Table X; for each structure, we give the Kanamori symbol,<sup>102</sup> the number of atoms per cell, and its description as a superlattice. One observes that the chalcopyrite phase (CH), and two phases with composition  $x = \frac{1}{4}$  and  $\frac{1}{5}$ , all [201] superlattices, belong to the ground state of all lattice-mismatched systems.

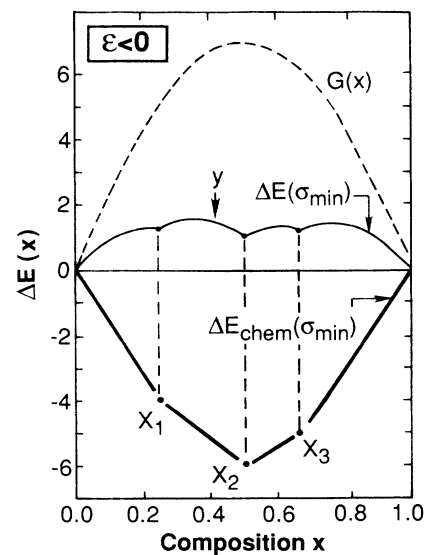


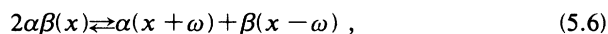
FIG. 17. Schematic plot of the chemical ground-state line  $\Delta E_{\text{chem}}(\sigma_{\text{min}})$  [see Eq. (5.1)], the elastic energy  $G(x)$ , and their sum  $\Delta E(\sigma_{\text{min}})$ . Note that at compositions “ $y$ ” between vertex points of  $\Delta E_{\text{chem}}(\sigma_{\text{min}})$  the system can lower its energy by local decomposition, whereas the vertices points  $X_1$ ,  $X_2$ , and  $X_3$  are locally stable with respect to decomposition and will hence produce metastable long-range ordering.

TABLE X. Ordered configurations corresponding to vertices in the ground-state line of chemical energy  $\Delta E_{\text{chem}}(\sigma)$ . All configurations with up to 15 atoms/cell were considered. These configurations are superlattices with alternating planes ( $p, q, r, \dots$ ), that is,  $p$  planes of  $B$ ,  $r$  planes of  $A$  followed by  $q$  planes of  $A$ , etc., along the direction  $[l, m, n]$ . An "X" symbol in the last six columns indicates that the corresponding phase is a ground state.

$x$	Our symbol	Kanamori symbol (Ref. 100)	Superlattice description	Atoms per cell	GaSb		GaP		InAs		HgTe		CdTe	
					GaAs	GaAs	InP	GaAs	GaAs	ZnTe	ZnTe			
$\frac{1}{13}$		$[0,0,0,0;\frac{1}{13}]$	(12,1) [9,3,1]	13	X				X					
$\frac{1}{6}$		$[0,1,0,0;\frac{1}{6}]$	(8,1) [3,1,0] or [9,3,1]	9			X		X			X		X
$\frac{1}{7}$		$[0,0,3,0;\frac{1}{7}]$	(6,1) [5,3,1]	7	X									
$\frac{1}{5}$		$[0,1,4,0;\frac{1}{5}]$	(4,1) [2,1,0]	5	X		X		X			X		X
$\frac{1}{4}$		$[\frac{1}{2},1,5,0;\frac{1}{4}]$	(4,1,2,1) [2,1,0]	8	X		X		X			X		X
$\frac{2}{7}$		$[\frac{3}{4},1,\frac{21}{4},\frac{1}{2};\frac{2}{7}]$	(3,1,4,1,3,2) [7,5,1]	14	X				X					
		$[\frac{1}{2},\frac{3}{2},5,1;\frac{2}{7}]$	(3,1,2,1) [2,1,0]	7			X					X		X
$\frac{1}{3}$	C1	$[1,1,6,1;\frac{1}{3}]$	(2,1) [1,1,0] or [2,1,0]	3		X								
		$[1,\frac{3}{2},\frac{11}{2},1;\frac{1}{3}]$	(4,1,1,1,2,1,1) [3,1,0]	12			X		X			X		X
$\frac{2}{5}$		$[\frac{3}{2},\frac{3}{2},6,\frac{3}{2};\frac{2}{5}]$	(3,2) [2,1,0]	5		X		X		X				
$\frac{5}{12}$		$[\frac{8}{5},\frac{9}{5},\frac{32}{5},\frac{8}{5};\frac{5}{12}]$	(3,1,2,2,2,2) [3,2,0]	12			X		X			X		X
$\frac{1}{2}$	CH	$[2,2,8,2;\frac{1}{2}]$	(2,2) [2,1,0]	4		X		X		X		X		X

For the purpose of a qualitative discussion, we show in Fig. 17 a schematic and simplified version of the ground-state line  $\Delta E_{\text{chem}}(\sigma_{\min})$  with just three vertices. Note that only when  $\varepsilon < 0$  do we find a nontrivial ground-state line, while when  $\varepsilon > 0$ , as is the case in lattice-matched alloys, the ground-state line is purely horizontal at the  $E=0$  level. Clearly, no ordering is possible in this case.

(ii) *Heterogeneous equilibrium search*: In the second step we consider the possibility of decomposition of a phase  $\alpha\beta$  into two phases of *different* compositions, e.g.,



where  $\omega$  is an infinitesimal composition change. In this case the elastic energy  $G(x)$  is included. Figure 17 shows schematically  $G(x)$ , and the sum  $\Delta E(\sigma_{\min})$  of  $G(x)$  with the ground-state line  $\Delta E_{\text{chem}}(\sigma_{\min})$  as a solid line. For size-mismatched semiconductors the positive elastic energy  $G(x)$  overwhelms the negative chemical energy; since the sum of these two contributions,  $\Delta E(\sigma_{\min})$ , is non-negative for all  $x$ 's, the ground state at  $T=0$  K corresponds to a mixture of the pure binary constituents. However, a local minimum can exist. This can be seen by considering a composition  $y$  *between* two vertices of the ground-state line (say, 1 and 2 in Fig. 17). In this case the energy change associated with reaction (5.6) is purely elastic, i.e.,

$$\delta \Delta E = G(y+\omega) + G(y-\omega) - 2G(y) = \omega^2 \frac{d^2 G}{dx^2} \Big|_{x=y}. \quad (5.7a)$$

Since by use of Eq. (4.12),  $d^2 G/dx^2 = -Z(x)$ , where  $Z(x) > 0$  by Eq. (4.7), this energy change must be negative, i.e.,

$$\delta \Delta E = -\omega^2 Z(y) < 0, \quad (5.7b)$$

and the reaction (5.6) proceeds to the right (decomposition). This process can continue until one reaches a composition  $x$  corresponding to a vertex in the ground-state line surrounded by two minima (e.g., vertex 2 surrounded by vertices 1 and 3 in Fig. 17). Now the energy change

associated with reaction (5.6) has both elastic and chemical contributions. By use of Eqs. (5.1)–(5.5), we have

$$\delta \Delta E = -\omega^2 Z(x) + \omega \left[ \frac{\varepsilon^{(3)} - \varepsilon^{(2)}}{X_3 - X_2} - \frac{\varepsilon^{(2)} - \varepsilon^{(1)}}{X_2 - X_1} \right]. \quad (5.8)$$

Since the second term (“chemical”) is positive and linear in the concentration fluctuation  $\omega$ , it will overwhelm the elastic term (quadratic in  $\omega$ ) for small  $\omega$ . In this case  $\delta \Delta E$  is positive and reaction (5.6) proceeds to the left: compound formation is favored. Hence, the local minima of  $\Delta E(\sigma_{\min})$  (Fig. 17 and Table X) correspond to metastable long-range ordering. We conclude that at a general composition  $x$ , phase separation will occur until a special composition  $X_2$  is encountered, at which point  $\Delta E(X_2)$  becomes locally stable against composition fluctuations. In perfect equilibrium at  $X_2$  the system will overcome the barriers evident in Fig. 17 and produce the true phase-separated ground state. However, at sufficiently low temperatures the system cannot surmount these barriers and will exhibit long-range ordering in the phases shown in Table X. This demonstrates that metastable long-range ordering found in our phase-diagram calculations is a consequence of the coexistence of negative chemical energies with (larger), positive elastic energies.

Having identified the ground-state structures, it remains to be seen whether the stability-limit temperature given by  $d^2 F/dx^2 = 0$  is sufficiently high to allow growth of these ordered phases. For this purpose, we constructed a CVM-correlation-function computer program able to calculate the free energy of any fcc-based structure specified by its unit vectors. The input to the program is only the triad of unit vectors and the occupation (with  $A$  or  $B$ ) of its sublattices. The program itself generates the space group, determines the independent figures, finds the Kikuchi coefficients<sup>44</sup> for the CVM entropy expansion using Barker's procedure,<sup>46</sup> finds the linear relations between reduced density matrix elements and correlation functions, and determines how the non-first-neighbor pair correlations decouple into products of point figure correlations. Applications of this procedure to the ground-state structures of Table X provides their

TABLE XI. Limiting temperature  $T_c$  of stability for some GaSbAs phases belonging to the ground-state line of chemical energies. Calculations were made with Eq. (4.10). We characterize each structure by the number and type of independent figures appearing in it. Here,  $Q$  means a tetrahedron,  $T$  a triangle,  $P1$  a first-neighbor pair,  $D$  a point, and  $P2$ ,  $P3$ , and  $P4$  second-, third-, and fourth-neighbor pairs.

$x$	Our symbol	Kananori symbol (Ref. 100)	Atoms per Cell	Independent figures	$T_c$ (K)
$\frac{1}{5}$		$[0, 1, 4, 0; \frac{1}{5}]$	5	$2Q + 3T + 3P1 + 2D + 3P2 + 3P3 + 2P4$	123
$\frac{1}{4}$		$[\frac{1}{2}, 1, 5, 0; \frac{1}{4}]$	8	$5Q + 12T + 14P1 + 4D + 10P2 + 10P3 + 6P4$	137
$\frac{1}{3}$	C1	$[1, 1, 6, 1; \frac{1}{3}]$	3	$2Q + 4T + 4P1 + 2D + 3P2 + 3P3 + 3P4$	153
$\frac{2}{5}$		$[\frac{3}{2}, \frac{3}{2}, 6, \frac{3}{2}; \frac{2}{5}]$	5	$3Q + 6T + 6P1 + 3D + 6P2 + 6P3 + 5P4$	172
$\frac{1}{2}$	CH	$[2, 2, 8, 2; \frac{1}{2}]$	4	$1Q + 2T + 4P1 + 2D + 3P2 + 3P3 + 3P4$	287
$\frac{3}{5}$		$[\frac{3}{2}, \frac{3}{6}, 6, \frac{3}{2}; \frac{3}{5}]$	5	$3Q + 6T + 6P1 + 3D + 6P2 + 6P3 + 5P4$	178
$\frac{2}{3}$	C2	$[1, 1, 6, 1; \frac{2}{3}]$	3	$2Q + 4T + 4P1 + 2D + 3P2 + 3P3 + 3P4$	165
$\frac{3}{4}$		$[\frac{1}{2}, 1, 5, 0; \frac{3}{4}]$	8	$5Q + 12T + 14P1 + 4D + 10P2 + 10P3 + 6P4$	145
$\frac{4}{5}$		$[0, 1, 4, 0; \frac{4}{5}]$	5	$2Q + 3T + 3P1 + 2D + 3P2 + 3P3 + 2P4$	140

free energies  $\Delta F(x, T)$  from which the stability limit is calculated.

In Table XI we present the stability-limit temperature for phases belonging to the ground-state line of GaSbAs. We see that these stability temperatures are well below current growth temperatures. Other effects (e.g., surface reconstruction) may modify these ordering temperatures.

## VI. EFFECTS OF PRESSURE

The results discussed so far are for zero pressure. For any configuration  $\sigma$  under a hydrostatic pressure  $p$ , the volume- and pressure-dependent enthalpy is given by

$$E(\sigma, p, V) = E(\sigma, V) + pV, \quad (6.1)$$

where  $E(\sigma, V)$  is the volume-dependent internal energy. At equilibrium the enthalpy is

$$H(\sigma, p) = E[\sigma, V(\sigma, p)] + pV(\sigma, p), \quad (6.2)$$

where  $V(\sigma, p)$  is the equilibrium volume at pressure  $p$ . Noticing that, from Eq. (6.2),

$$\frac{dH(\sigma, p)}{dp} = V(\sigma, p), \quad (6.3)$$

one can write

$$H(\sigma, p) = H(\sigma, 0) + \int_0^p V(\sigma, p') dp'. \quad (6.4)$$

Equation (6.4) provides a convenient way to relate the enthalpy at pressure  $p$  to that at zero pressure.

### A. The equation-of-state approach

In the case where the internal energy is written as a linear combination of the energies of special configurations [Eq. (2.7)], we can write

$$E(\sigma, p, V) = \sum_s^{N_s} \xi_s(\sigma) E(s, p, V), \quad (6.5)$$

where, from Eq. (6.1) for  $\sigma = s$ ,

$$E(s, p, V) = E(s, V) + pV. \quad (6.6)$$

Equations (6.5) and (6.6) can be easily implemented into the current program (see Sec. II) by simply adding the term  $pV$  to the equation of state (EOS) (e.g., Ref. 58).

Figure 18 depicts the calculated results for GaAs<sub>x</sub>Sb<sub>1-x</sub>, where we show the calculated phase diagram of  $p=0$  and 30 Gpa, and indicate how the critical points ( $T_{MG}, X_{MG}$ ) move with pressure (dashed line). In this calculation we have used the numerically calculated  $\bar{\epsilon}_n[V, x, p]$  rather than its fitted form.<sup>59</sup> The results (Fig. 18) show that under pressure the miscibility-gap temperature  $T_{MG}$  increases and the position of the critical point  $X_{MG}$  shifts towards the constituents with the larger volume (GaSb). This and other qualitative trends with pressure can be conveniently discussed within the  $\epsilon$ - $G$  approach, as follows.

### B. $\epsilon$ - $G$ approach

The pressure dependence of the enthalpy of Eq. (6.4) can be expressed in the  $\epsilon$ - $G$  model (Sec. IV B) as

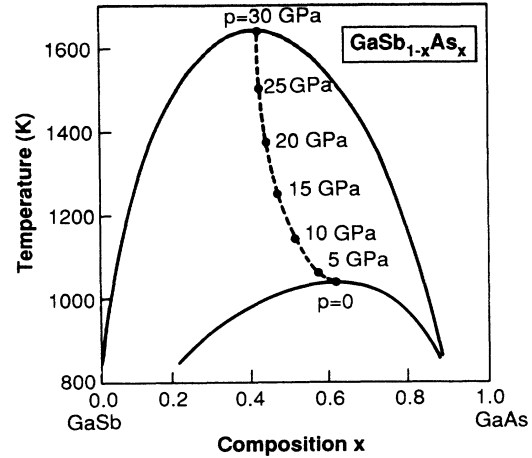


FIG. 18. Calculated [Eqs. (6.5) and (6.6)] pressure dependence of the phase diagram of GaSb<sub>1-x</sub>As<sub>x</sub>. The dashed line indicates the position of the top of the miscibility gap as a function of pressure.

$$H(\sigma, p) = [\epsilon(\sigma) + G(x)] + \int_0^p V(x, p') dp'. \quad (6.7)$$

The first two terms in square brackets are  $H(\sigma, 0)$  of Eq. (4.1). The last term can be expanded in a power series of pressure to give

$$H(\sigma, p) = [\epsilon(\sigma) + G(x)] + pV(x, 0) - \frac{p^2}{2} \frac{V(x, 0)}{B(x, 0)} + \dots \quad (6.8)$$

Recalling that, by definition,

$$\epsilon(A) = \epsilon(B) = 0, \quad (6.9)$$

$$G(0) = G(1) = 0$$

for the pure material ( $x=0,1$ ), the mixing enthalpy then becomes

$$\Delta H(\sigma, p) = [\epsilon(\sigma) + G(x)] + p \Delta V(x, 0) - \frac{p^2}{2} \Delta \left[ \frac{V(x, 0)}{B(x, 0)} \right] + \dots, \quad (6.10)$$

for  $A_{1-x}B_x$ , and

$$\Delta V = V(x, 0) - xV(1, 0) - (1-x)V(0, 0), \quad (6.11a)$$

$$\Delta(V/B) = \frac{V(x, 0)}{B(x, 0)} - x \frac{V(1, 0)}{B(1, 0)} - (1-x) \frac{V(0, 0)}{B(0, 0)}. \quad (6.11b)$$

We conclude the following.

(i) The enthalpy difference  $H(\alpha, p) - H(\beta, p)$  of two homogeneous phases at constant pressure and composition does not depend, in lowest order, on the pressure. Hence, the  $\alpha \rightarrow \beta$  transition (e.g., order  $\rightarrow$  disorder) temperature depends but weakly on  $p$ .

(ii) In phase-separating alloys,  $\Delta H(\sigma, p)$  and  $T_{MG}(p)$  depend on pressure linearly at low  $p$ , through  $p \Delta V(x, 0)$ : positive (negative) deviations from Vegard's rule<sup>103</sup> lead to increase (decrease) with  $p$ .

(iii) For systems obeying Vegard's rule<sup>103</sup> (e.g., most of

the isovalent semiconductor alloy) the change with pressure of  $\Delta H$  and  $T_{MG}$  following the bowing [Eq. (6.11b)] of  $V/B$ . At low  $p$  the change is very slow because it depends quadratically on  $p$ .

To have a more qualitative understanding of this change, we use Eq. (3.4) to describe the change of  $V(x)$  and  $B(x)$ . In this case

$$\Delta \left[ \frac{V(x)}{B(x)} \right] = \frac{V_A + x \delta V}{B_A + x \delta B} - (1-x) \frac{V_A}{B_A} - x \frac{V_A + \delta V}{B_A + \delta B} \\ = \frac{\delta B(B_A \delta V - V_A \delta B)}{B_A(B_A + x \delta B)(B_A + \delta B)} x(1-x). \quad (6.12)$$

where  $\delta V = V_B - V_A$  and  $\delta B = B_B - B_A$ . For semiconductors the bulk modulus  $B$  is a decreasing function of volume  $V$  (i.e.,  $\delta V/\delta B < 0$ ), and hence  $\Delta[V(x)/B(x)]$  is always negative. This means that  $\Delta H$  and  $T_{MG}$  are increasing functions of  $p$  [see Eq. (6.10)]. Furthermore, Eq. (6.12) is asymmetric relative to  $x = \frac{1}{2}$ . It has a minimum at  $X_{min}$  which is closer to the constituents with small bulk modulus (larger volume for semiconductors). This suggests that  $X_{MG}$  will shift towards  $X_{min}$  with increasing pressure. The discussion above explains the trend of phase boundary as a function of pressure depicted in Fig. 18 (dashed line) for  $\text{GaSb}_{1-x}\text{As}_x$ .

Other phase-diagram calculations with pressure<sup>104,105</sup> have been reported for the  $\text{Ge}_{1-x}\text{Si}_x$  system. Similar trends (i.e., increased  $T_{MG}$  and shift of  $X_{MG}$  towards Ge under pressure) were observed.

## VII. SUMMARY

Our study suggests that the thermodynamic properties of bulk isovalent zinc-blende semiconductor alloys can be qualitatively understood in terms of a general Ising model with up to fourth-neighbor interactions and that the LDA forms an adequate basis for self-consistently describing those interactions. The global trends can be understood by separating [Eq. (4.10)] the excess enthalpy  $\Delta H(x, T)$  into a volume- (or composition-) dependent term  $G(x)$ , reflecting microscopic size mismatch, and a sum over volume-independent configurational (or substitutional) energies  $\epsilon$  reflecting events at constant molar volume, i.e., sublattice relaxation and charge redistribution. The alloys studied then naturally separate into the following two groups.

*Size-matched alloys* ( $\text{Al}_{1-x}\text{Ga}_x\text{As}$  and  $\text{Cd}_{1-x}\text{Hg}_x\text{Te}$ ): Here,  $G(x) \cong 0$  and, owing to negligible sublattice relaxation and unfavorable charge redistribution the substitutional energies  $\epsilon$  are (slightly) positive. This leads to the following characteristics.

(i) The disordered alloy has a lower excess enthalpy than any of the short-period ordered structures, reflecting the fact that for positive  $\epsilon$ 's a *superposition* of clusters has a lower energy than a *single* cluster. Hence these systems will appear as disordered alloys above  $T_{MG}$  and will phase-separate into their constituents below it. No metastable long-range ordering occurs.

(ii) Above  $T_{MG}$  the systems exhibit enhancement in the

populations of the pure  $A_4$  and  $B_4$  clusters and a depletion of the mixed clusters ("clustering"), again reflecting  $\epsilon > 0$ .

(iii) The mixing enthalpies are small and positive reflecting  $G \gtrsim 0$  and  $\epsilon > 0$ .

*Size-mismatched alloys* ( $\text{GaAs}_{1-x}\text{P}_x$ ,  $\text{In}_{1-x}\text{Ga}_x\text{P}$ ,  $\text{In}_{1-x}\text{Ga}_x\text{As}$ ,  $\text{GaSb}_{1-x}\text{As}_x$ ,  $\text{Cd}_{1-x}\text{Zn}_x\text{Te}$ , and  $\text{Hg}_{1-x}\text{Zn}_x\text{Te}$ ): Here,  $G(x) > 0$  owing to the  $A$ - $B$  size mismatch, yet  $\epsilon < 0$ , predominantly due to an effective sublattice relaxation which leads to bond alternation and a partial accommodation of strain. This leads to the following characteristics.

(i) Like size-matched alloys, size-mismatched alloys also have  $\Delta H(x, T) > 0$ , and hence at  $T=0$  they will phase-separate when perfect equilibrium is achieved. However, if phase separation is slow, long-range ordering will occur in the structures identified in Table X at the temperatures predicted in Tables VI and XI. These special arrangements have a lower enthalpy than the disordered alloy of the same composition. These conclusions pertain to *bulk* growth (e.g., liquid-phase epitaxy, or other melt techniques) since we have addressed in this work the thermodynamics of three-dimensionally coordinated atoms. Growth techniques involving a *free surface* (e.g., molecular-beam epitaxy) would have a different thermodynamics owing to the lower symmetry (e.g., surface clusters are likely to have different energies than clusters surrounded by atoms in all three directions). Indeed, in the presence of surface-reconstruction effects the energy-minimizing structure can be qualitatively different than that obtained by minimizing the *bulk* energy. To the extent that coverage of the surface freezes in the *surface* stable structure, it could persist metastably to macroscopic dimensions. The fact that growth techniques which involve free surfaces exhibit CuPt ordering<sup>67-78</sup> is, most likely, a reflection of this surface thermodynamic effect.

(ii) Above  $T_{MG}$ , lattice-mismatched systems will exhibit an excess of the mixed ( $A_3B$ ,  $A_2B_2$ , and  $AB_3$ ) clusters and a deficiency in the "pure" ( $A_4$  and  $B_4$ ) clusters ("anticlustering").

(iii) Their excess enthalpies reflect largely strain effects and, hence, approximately scale with the relative size mismatch  $|a_A - a_B|/|a_A + a_B|$ . These enthalpies are temperature dependent due to the pronounced temperature dependence of the cluster probabilities.

We conclude by contrasting our conclusions with those reached by their alloy models.

In classic models, based on *constant* interaction energies, alloys are broadly classified into two groups.

(i) Alloys for which  $\Delta H(x, T)$  in the disordered phase is known to be positive are said to be characterized by repulsive interactions. This is said to lead to clustering in the disordered phase and, at sufficiently low temperature, to phase separation. Repulsive interactions and long-range ordering are taken to be mutually exclusive. All isovalent semiconductor alloys are said to belong to this class.

(ii) Alloys for which  $\Delta H(x, T)$  in the disordered phase can be negative are said to be characterized by attractive interactions. This is expected to lead to anticlustering in

the disordered phase and to long-range order at sufficiently low temperatures.

Our work shows that this classification is false: Alloys with  $\Delta H(x, T) > 0$  (all isovalent semiconductors) can show clustering and phase separation (when size matched) or anticlustering and metastable long-range ordering (when size mismatched). This reflects the fact that there are two distinct physical sources of  $\Delta H > 0$ :  $G(x)$  and  $\epsilon$ , which control different aspects of the thermodynamics.

*Note added in proof.* After the acceptance of this paper for publication, K. Ishida, T. Nomura, H. Tokunaga, H. Ohtani, and T. Nishizawa [J. Less-Common Met. **155**, 193 (1989)] have reported an experimental determination of the phase diagram of solid  $\text{In}_{1-x}\text{Ga}_x\text{P}$  alloys. They find a miscibility-gap temperature  $T_{\text{MG}} \approx 933$  K with a maximum of  $x_{\text{MG}} \approx 0.62$ , very close to our predictions [Table IV and Fig. 10(c)] of  $T_{\text{MG}} = 961$  K and  $x_{\text{MG}} = 0.676$ . This differs substantially from the predictions of Czyzyk *et al.*<sup>97(b)</sup> giving  $T_{\text{MG}} = 620$  K and  $x_{\text{MG}} \approx 0.15$ . Ishida *et al.* have also estimated the interaction parameter  $\Omega(x, T = 800$  K) of Eq. (3.7), finding 2.95, 3.56, and 4.17 kcal/mol for  $x = 0, \frac{1}{2}$ , and 1, respectively,

close to our predicted values (Table VI) of 2.92, 3.07, and 4.60 kcal/mol. Their suggested empirical model for the temperature coefficient of  $\Omega(x, T)$  produces a value of  $-0.48 \text{ cal mol}^{-1} \text{ K}^{-1}$  (not measured) which is of the opposite sign of what is expected from thermodynamic considerations:  $\Delta H(x, T)$  should increase with temperature (Figs. 4 and 6) as the alloy becomes more random. Our calculated value of the temperature coefficient is  $\sim 0.15 \text{ cal mol}^{-1} \text{ K}^{-1}$ . A direct calorimetric measurement of this quantity will be useful.

#### ACKNOWLEDGMENTS

We thank Dr. R. Dandrea for providing us the input data for the GaP-GaAs system and Dr. D. Wood for discussions on the pressure effects (Sec. VI). This work was supported by the Office of Energy Research (OER) [Division of Materials Sciences of the Office of Basic Energy Sciences (BES)], U.S. Department of Energy, under Contract No. DE-AC02-77CH00178. We are grateful for an OER-BES grant of computer time ("Grand Challenge") which made this work possible.

- <sup>1</sup>P. Hohenberg and W. Kohn, Phys. Rev. **136**, B864 (1964); W. Kohn and L. J. Sham, *ibid.* **140**, A1133 (1965).
- <sup>2</sup>O. Gunnarsson and B. I. Lundqvist, Phys. Rev. B **13**, 4274 (1976).
- <sup>3</sup>J. Ihm, A. Zunger, and M. L. Cohen, J. Phys. C **12**, 4409 (1979).
- <sup>4</sup>P. Bendt and A. Zunger, Phys. Rev. Lett. **50**, 1684 (1983).
- <sup>5</sup>O. H. Nielsen and R. M. Martin, Phys. Rev. B **32**, 3780 (1985).
- <sup>6</sup>S.-H. Wei and H. Krakauer, Phys. Rev. Lett. **55**, 1200 (1985), and references therein.
- <sup>7</sup>*Local Density Approximations in Quantum Chemistry and Solid State Physics*, edited by J. P. Dahl and J. Avery (Plenum, New York, 1984).
- <sup>8</sup>*The Electronic Structure of Complex Systems*, Vol. 113 of *NATO Advanced Study Institute, Series B: Physics*, edited by P. Phariseau and W. M. Temmerman (Plenum, New York, 1982).
- <sup>9</sup>*Electronic Structure, Dynamics and Quantum Structural Properties of Condensed Matter*, Vol. 121 of *NATO Advanced Study Institute, Series B: Physics*, edited by J. T. Devreese and P. Van Camp (Plenum, New York, 1984).
- <sup>10</sup>*Density Functional Methods in Physics*, Vol. 123 of *NATO Advanced Study Institute, Series B: Physics*, edited by R. M. Dreizler and J. da Providencia (Plenum, New York, 1983).
- <sup>11</sup>*Theory of the Inhomogeneous Electron Gas*, edited by S. Lundqvist and N. H. March (Plenum, New York, 1983).
- <sup>12</sup>J. W. D. Connolly and A. R. Williams, Phys. Rev. B **27**, 5169 (1983).
- <sup>13</sup>D. D. Johnson, D. M. Nicholson, F. J. Pinski, B. L. Gyorffy, and G. M. Stocks, Phys. Rev. Lett. **56**, 2088 (1986); G. M. Stocks and H. Winter, in *The Electronic Structure of Complex Systems*, edited by P. Phariseau and W. M. Temmerman (Plenum, New York 1982), p. 463.
- <sup>14</sup>K. Terakura, T. Oguchi, T. Mohri, and K. Watanabe, Phys. Rev. B **35**, 2169 (1987); S. Takizawa and K. Terakura, *ibid.* **39**, 5792 (1989).
- <sup>15</sup>K. M. Rabe and J. D. Joannopoulos, Phys. Rev. Lett. **59**, 570 (1987).
- <sup>16</sup>S.-H. Wei, A. A. Mbaye, L. G. Ferreira, and A. Zunger, Phys. Rev. B **36**, 4163 (1987); A. Zunger, S.-H. Wei, A. A. Mbaye, and L. G. Ferreira, Acta Metall. **36**, 2239 (1988); A. A. Mbaye, L. G. Ferreira, and A. Zunger, Phys. Rev. Lett. **58**, 49 (1987).
- <sup>17</sup>P. E. A. Turchi, G. M. Stocks, W. H. Butler, D. M. Nicholson, and A. Gonis, Phys. Rev. B **37**, 5982 (1988).
- <sup>18</sup>R. Podloucky, H. J. F. Jansen, X. Q. Guo, and A. J. Freeman, Phys. Rev. B **37**, 5478 (1988).
- <sup>19</sup>D. M. Wood and A. Zunger, Phys. Rev. Lett. **61**, 1501 (1988).
- <sup>20</sup>J. E. Bernard, L. G. Ferreira, S.-H. Wei, and A. Zunger, Phys. Rev. B **38**, 6338 (1988).
- <sup>21</sup>L. G. Ferreira, S.-H. Wei, and A. Zunger, Phys. Rev. B **40**, 3197 (1989).
- <sup>22</sup>C. Domb, in *Phase Transitions and Critical Phenomena*, edited by C. Domb and H. S. Green (Academic, London, 1974), Vol. 3, p. 357; D. M. Burley, *ibid.* Vol. 2, p. 329; K. Binder, Phys. Rev. Lett. **45**, 811 (1980).
- <sup>23</sup>D. de Fontaine, in *Solid State Physics*, edited by H. Ehrenreich, F. Seitz, and D. Turnbull (Academic, New York, 1979), Vol. 34, p. 73.
- <sup>24</sup>J. M. Sanchez, F. Ducastelle, and D. Gratias, Physica **128A**, 334 (1984).
- <sup>25</sup>D. M. Ceperley and B. J. Alder, Phys. Rev. Lett. **45**, 566 (1980); J. P. Perdew and A. Zunger, Phys. Rev. B **23**, 5048 (1981).
- <sup>26</sup>L. Hedin and B. I. Lundqvist, J. Phys. C **4**, 2063 (1971).
- <sup>27</sup>(a) D. J. Chadi and M. L. Cohen, Phys. Rev. B **8**, 5747 (1973); S. Froyen, *ibid.* **39**, 3168 (1989); (b) LAPW total-energy calculations for  $\text{GaInP}_2$ ,  $\text{GaInAs}_2$ , and  $\text{GaAlAs}_2$  in the CuAu-I structure using the equivalent of 10 zinc-blende-structure  $\mathbf{k}$  points give the formation enthalpies (in units of meV/four-atoms) 95.0, 67.5, and 13.8, respectively, while two- $\mathbf{k}$ -point calculations, used here, give 91, 66.7, and 11.5, respectively;

- see N. E. Christensen, S.-H. Wei, and A. Zunger, *Phys. Rev. B* **40**, 1642 (1989), where the 10- $k$ -point results for GaAlAs are used. Here and in Ref. 21 we use the two- $k$ -point results.
- <sup>28</sup>I. M. Torrence, *Interatomic Potentials* (Academic, New York, 1972); in *Computer Simulation of Solids*, Vol. 166 of *Lecture Notes in Physics*, edited by C. R. A. Catlow and W. C. Mackrodt (Springer-Verlag, Berlin, 1982).
- <sup>29</sup>M. Sluiter, P. Turchi, and D. de Fontaine, *J. Phys. F* **17**, 2163 (1987).
- <sup>30</sup>A. Berera, H. Dreysse, L. T. Wille, and D. de Fontaine, *J. Phys. F* **18**, L49 (1988); H. Dreysse, A. Berera, L. T. Wille, and D. de Fontaine, *Phys. Rev. B* **39**, 2442 (1989).
- <sup>31</sup>F. Ducastelle and F. Gautier, *J. Phys. F* **6**, 2039 (1976).
- <sup>32</sup>A. Bieber and F. Gautier, *Acta Metall.* **35**, 1839 (1987); **34**, 2291 (1986).
- <sup>33</sup>M. O. Robbins and L. M. Falicov, *Phys. Rev. B* **29**, 1333 (1984); D. G. Pettifor, *J. Phys. C* **5**, 97 (1972).
- <sup>34</sup>F. Cyrot-Lackmann, *J. Phys. Chem. Solids* **29**, 1235 (1968); M. Cyrot and F. Cyrot-Lackmann, *J. Phys. F* **6**, 2257 (1976).
- <sup>35</sup>J. Friedel, in *Physics of Metals*, edited by J. M. Ziman (Cambridge University Press, London, 1969).
- <sup>36</sup>M. Jaros, *Rep. Prog. Phys.* **48**, 1091 (1985); S.-H. Wei and A. Zunger, *Phys. Rev. B* **39**, 3279 (1989).
- <sup>37</sup>*JANAF Thermochemical Tables*, 3rd ed., edited by M. W. Chase, C. A. Davies, J. R. Downey, D. J. Frurip, R. A. McDonald, and A. N. Syverud (American Chemical Society, New York, 1986), Pts. I and II.
- <sup>38</sup>O. Kubaschewski and C. B. Alcock, *Metallurgical Thermochemistry* (Pergamon, Oxford, 1979).
- <sup>39</sup>R. Hultgren, P. D. Desai, D. T. Hawkins, M. Gleiser, and K. K. Kelley, *Selected Values of the Thermodynamic Properties of Binary Alloys* (American Society for Metals, Metals Park, OH, 1973).
- <sup>40</sup>(a) J. C. Mikkelsen and J. B. Boyce, *Phys. Rev. Lett.* **49**, 1412 (1982); (b) C. Y. Fong, W. Weber, and J. C. Phillips, *Phys. Rev. B* **14**, 5387 (1976).
- <sup>41</sup>A. Mbaye, D. M. Wood, and A. Zunger, *Phys. Rev. B* **37**, 3008 (1988).
- <sup>42</sup>R. Kikuchi, J. M. Sanchez, D. de Fontaine, and H. Yamauchi, *Acta Metall.* **28**, 651 (1980).
- <sup>43</sup>N. Metropolis, A. W. Rosenbluth, M. N. Rosenbluth, A. Teller, and E. Teller, *J. Chem. Phys.* **21**, 1087 (1953).
- <sup>44</sup>R. Kikuchi, *J. Chem. Phys.* **60**, 1071 (1974); *Phys. Rev.* **81**, 988 (1951).
- <sup>45</sup>C. G. Broyden, *Math. Comput.* **19**, 577 (1965).
- <sup>46</sup>J. A. Barker, *Proc. R. Soc. London* **216**, 45 (1953).
- <sup>47</sup>T. Morita, *J. Phys. Soc. Jpn.* **12**, 753 (1957).
- <sup>48</sup>A. Finel and F. Ducastelle, *Europhys. Lett.* **1**, 135 (1986), and unpublished results.
- <sup>49</sup>R. G. Dandrea, J. E. Bernard, S.-H. Wei, and A. Zunger, *Phys. Rev. Lett.* **64**, 36 (1990).
- <sup>50</sup>J. S. Nelson and J. P. Batra, *Phys. Rev. B* **39**, 3250 (1989).
- <sup>51</sup>P. Boguslawski and A. Baldereschi, *Solid State Commun.* **66**, 679 (1988); *Phys. Rev. B* **39**, 8055 (1989).
- <sup>52</sup>T. Ohno, *Phys. Rev. B* **38**, 13 191 (1988).
- <sup>53</sup>A. Qteish, N. Motta, and A. Balzarotti, *Phys. Rev. B* **39**, 5987 (1989).
- <sup>54</sup>D. M. Bylander and L. Kleinman, *Phys. Rev. B* **36**, 3229 (1987).
- <sup>55</sup>K. C. Hass and D. Vanderbilt, *J. Vac. Sci. Technol. A* **5**, 3019 (1987); in *Proceedings of the 18th International Conference on the Physics of Semiconductors*, edited by O. Engström (World Scientific, Singapore, 1987), p. 1181.
- <sup>56</sup>H. E. Casey, Jr. and F. A. Trumbore, *Mater. Sci. Eng.* **6**, 69 (1979). Data for II-VI compounds were collected in Ref. 57.
- <sup>57</sup>S.-H. Wei and A. Zunger, *Phys. Rev. B* **37**, 8958 (1988).
- <sup>58</sup>F. D. Murnaghan, *Proc. Nat. Acad. Sci. U.S.A.* **30**, 244 (1944).
- <sup>59</sup>In this work the effective equations of state  $\bar{\epsilon}_n(V(x))$  were also fitted to Murnaghan's equation of state (EOS), and the fitted EOS are used in the phase-diagram calculations. We find that this procedure introduced only small errors. For example, for GaSb<sub>1-x</sub>As<sub>x</sub>, with the fitting the calculated miscibility-gap (MG) temperature  $T_{MG}$  and composition  $X_{MG}$  are 1080 K and 0.595, respectively, compared with  $T_{MG} = 1037$  K and  $X_{MG} = 0.613$  using numerical data of  $\bar{\epsilon}_n$  (i.e., without fitting).
- <sup>60</sup>H. Nakayama and H. Fujita, in *Proceedings of the 12th International Symposium on GaAs and Related Compounds*, Karuizawa, 1985, Inst. Phys. Conf. Ser. No. 79, edited by M. Fujimoto (IOP, London, 1986), p. 289.
- <sup>61</sup>H. R. Jen, M. J. Cherng, and G. B. Stringfellow, *Appl. Phys. Lett.* **48**, 1603 (1986).
- <sup>62</sup>H. R. Jen, M. J. Cherng, and G. B. Stringfellow, *J. Cryst. Growth* **85**, 175 (1987).
- <sup>63</sup>H. R. Jen, M. J. Cherng, M. J. Jou, and G. B. Stringfellow, in *Proceedings of the 13th International Symposium on GaAs and Related Compounds*, Inst. Phys. Conf. Ser. No. 83, edited by W. T. Lindley (IOP, London, 1987), p. 159.
- <sup>64</sup>T. S. Kuan, T. F. Kuech, W. I. Wang, and E. L. Wilkie, *Phys. Rev. Lett.* **54**, 201 (1985).
- <sup>65</sup>A. G. Norman, R. E. Mallard, I. J. Murgatroyd, and G. R. Brooker, A. H. Moore, and M. D. Scott, in *Microscopy of Semiconducting Materials, 1987*, Inst. Phys. Conf. Ser. No. 87, edited by A. G. Cullis and P. A. Augustus (IOP, London, 1987), p. 77.
- <sup>66</sup>I. J. Murgatroyd, A. G. Norman, G. R. Booker, and T. M. Kerr, in *Proceedings of the 11th International Conference on Electron Microscopy*, Kyoto, 1986, edited by T. Imura, S. Maruse, and T. Suzuki (Japan Society of Electron Microscopy, Tokyo, 1986), p. 1497.
- <sup>67</sup>Y. E. Ihm, N. Otsuka, J. Klen, and H. Morkoç, *Appl. Phys. Lett.* **51**, 2013 (1987).
- <sup>68</sup>A. Gomyo, T. Suzuki, K. Kobayashi, S. Kawata, and I. Hino, *Appl. Phys. Lett.* **50**, 673 (1987).
- <sup>69</sup>A. Gomyo, T. Suzuki, and S. Iijima, *Phys. Rev. Lett.* **60**, 2645 (1988).
- <sup>70</sup>A. Gomyo, K. Kobayashi, S. Kawata, I. Hino, and T. Suzuki, *J. Cryst. Growth* **77**, 367 (1986).
- <sup>71</sup>S. McKernan, B. C. DeCooman, C. B. Carter, D. P. Bour, and J. R. Shealy, *J. Mater. Res.* **3**, 406 (1988).
- <sup>72</sup>M. Kondow, H. Kakibayashi, and S. Minagawa, *J. Cryst. Growth* **88**, 291 (1988).
- <sup>73</sup>P. Bellon, J. P. Chevalier, G. P. Martin, E. DuPont-Nivet, C. Thiebaut, and J. P. André, *Appl. Phys. Lett.* **52**, 567 (1988).
- <sup>74</sup>O. Keda, M. Takikawa, J. Komeno, and I. Umebu, *Jpn. J. Appl. Phys.* **26**, L1824 (1987).
- <sup>75</sup>S. R. Kurtz, J. M. Olson, and A. Kibbler, *Solar Cells* **24**, 307 (1988); J. P. Goral, M. M. Al-Jassim, J. M. Olson, and A. Kibbler, in *Epitaxy of Semiconductor Layered Structures*, Vol. 102 of *Materials Research Society Symposium Proceedings*, edited by R. T. Tung, L. R. Dawson, and R. L. Gunshor (MRS, Pittsburgh, 1988), p. 583.
- <sup>76</sup>T. Nishino, Y. Inoue, Y. Hamakawa, M. Knodow, and S. Minagawa, *Appl. Phys. Lett.* **52**, 583 (1988).
- <sup>77</sup>M. A. Shahid, S. Mahajan, D. E. Laughlin, and H. M. Cox, *Phys. Rev. Lett.* **58**, 2567 (1987).
- <sup>78</sup>M. A. Shahid and S. Mahajan, *Phys. Rev. B* **38**, 1344 (1988).
- <sup>79</sup>L. M. Foster, J. E. Scardefield, and J. F. Woods, *J. Electro-*

- chem. Soc. **119**, 765 (1972).
- <sup>80</sup>M. B. Panish and M. Ilegems, *Prog. Solid State Chem.* **7**, 39 (1972).
- <sup>81</sup>G. B. Stringfellow, *J. Cryst. Growth* **27**, 21 (1974); **58**, 194 (1982).
- <sup>82</sup>L. M. Foster, J. E. Scardefield, and J. F. Woods, *J. Electrochem. Soc.* **119**, 1426 (1972).
- <sup>83</sup>G. A. Antypas, *J. Electrochem. Soc.* **117**, 700 (1970).
- <sup>84</sup>L. M. Foster and J. F. Woods, *J. Electrochem. Soc.* **118**, 1175 (1971).
- <sup>85</sup>L. M. Foster (unpublished).
- <sup>86</sup>A. Laugies, *Rev. Phys. Appl.* **8**, 259 (1973).
- <sup>87</sup>C. H. Su, P. K. Liao, and R. F. Brebrick, *J. Electrochem. Soc.* **132**, 942 (1985). Value taken at  $T=1000$  K.
- <sup>88</sup>R. F. Brebrick and R. J. Panlener, *J. Electrochem. Soc.* **121**, 932 (1974).
- <sup>89</sup>G. B. Stringfellow, *J. Phys. Chem. Solids* **34**, 1749 (1973).
- <sup>90</sup>J. L. Martins and A. Zunger, *Phys. Rev. B* **30**, 6217 (1984).
- <sup>91</sup>A. Sher, M. Van Schilfgaarde, A. B. Chen, and W. Chen, *Phys. Rev. B* **36**, 4279 (1987).
- <sup>92</sup>J. C. Woolley, in *Compound Semiconductors*, edited by R. K. Willardson and H. L. Goering (Reinhold, London, 1962), p. 3; K. J. Bachmann, F. A. Thiel, and H. Schreiber, *Prog. Cryst. Growth Charact.* **2**, 171 (1979); E. Lendvay, *Prog. Cryst. Growth Charact.* **8**, 371 (1984).
- <sup>93</sup>K. Ishida, T. Shumiya, T. Nomura, H. Ohtani, and T. Nishizawa, *J. Less-Common Met.* **142**, 135 (1988).
- <sup>94</sup>M. F. Grattton and J. C. Woolley, *J. Electrochem. Soc.* **127**, 55 (1980); *J. Electron. Mater.* **2**, 455 (1973); also see M. F. Grattton, R. C. Goodchild, L. Y. Juravel, and J. C. Woolley, *J. Electron. Mater.* **8**, 25 (1979).
- <sup>95</sup>V. T. Bublik, M. B. Karman, V. F. Klepstein, and V. N. Leikin, *Phys. Status Solidi A* **32**, 631 (1975); V. T. Bublik and V. N. Leikin, *ibid.* **46**, 365 (1978).
- <sup>96</sup>(a) G. B. Stringfellow, *J. Cryst. Growth* **58**, 194 (1982); (b) *J. Appl. Phys.* **54**, 404 (1983); (c) *J. Electron. Mater.* **11**, 903 (1982).
- <sup>97</sup>(a) P. Letardi, N. Motta, and A. Balzarotti, *J. Phys. C* **20**, 2853 (1987); (b) M. T. Czyzyk, M. Podgorny, A. Balzarotti, P. Letardi, N. Motta, A. Kisiel, and M. Zimnal-Starnawska, *Z. Phys. B* **62**, 153 (1986).
- <sup>98</sup>L. G. Ferreira, A. A. Mbaye, and A. Zunger, *Phys. Rev. B* **37**, 10 547 (1988).
- <sup>99</sup>D. F. Styre, M. K. Phani, and J. Lebowitz, *Phys. Rev. B* **34**, 3361 (1986).
- <sup>100</sup>W. L. Bragg and E. J. Williams, *Proc. R. Soc. London, Ser. A* **145**, 699 (1934).
- <sup>101</sup>S. M. Allen and J. W. Cahn, *Acta Metall.* **20**, 423 (1973); also see M. J. Richards and J. W. Cahn, *ibid.* **19**, 1263 (1971).
- <sup>102</sup>J. Kanamori and Y. Kakehashi, *J. Phys. (Paris) Colloq.* **38**, C7-274 (1977); J. Kanamori, in *Modulated Structures 1979*, edited by J. M. Cowley, J. B. Cohen, M. B. Salamon, and B. J. Wuensch (AIP, New York, 1979), p. 117.
- <sup>103</sup>L. Vegard, *Z. Phys.* **5**, 17 (1921).
- <sup>104</sup>H. M. Kagaya and T. Soma, *Phys. Status Solidi B* **144**, 549 (1987).
- <sup>105</sup>A. Qteish and R. Resta, *Phys. Rev. B* **37**, 6483 (1988).

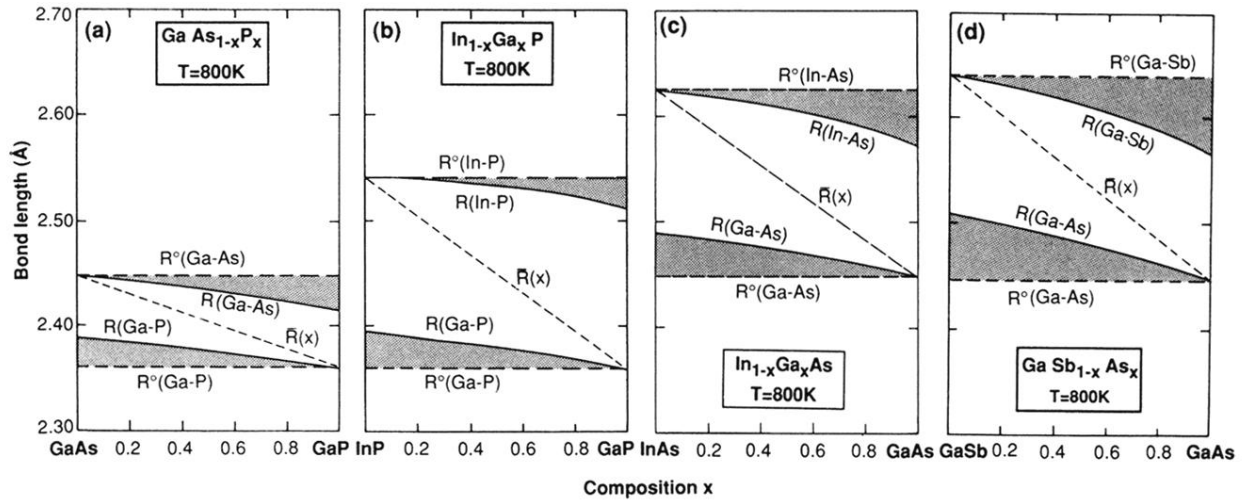


FIG. 12. Calculated equilibrium alloy bond lengths  $R(A-C)$  and  $R(B-C)$  at  $T=800$  K (solid lines), compared with the “ideal” zinc-blende values  $R^0(A-C)$  and  $R^0(B-C)$  (dashed horizontal lines). The composition-weighted average  $\bar{R}(x)$  is given for comparison. The shaded areas represent deviations of equilibrium alloy bond lengths from the “ideal” values. The strain, frozen-in due to such deviations leads to  $\Delta H > 0$ . Results are given for the size-matched III-V alloys (a)  $\text{GaAs}_{1-x}\text{P}_x$  (b)  $\text{In}_{1-x}\text{Ga}_x\text{P}$ , (c)  $\text{In}_{1-x}\text{Ga}_x\text{As}$ , and (d)  $\text{GaSb}_{1-x}\text{As}_x$ .

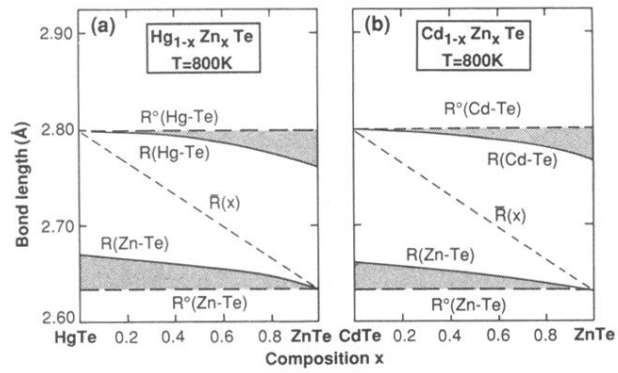


FIG. 13. Like Fig. 12 (see caption), but for the II-VI size-mismatched alloys (a)  $\text{Hg}_{1-x}\text{Zn}_x\text{Te}$  and (b)  $\text{Cd}_{1-x}\text{Zn}_x\text{Te}$ .

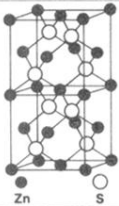
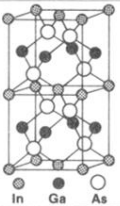
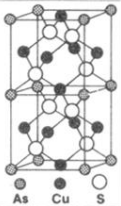
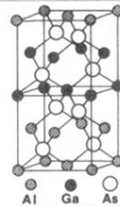
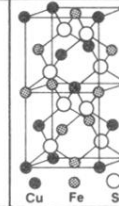
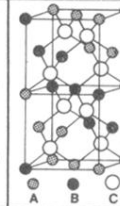
Ordering Vector	(0,0,0)	(0,0,1)			(2,0,1)	(1,1,1)
Name	Zincblende (Sphalerite)	Layered tetragonal	"Luzonite"	2 layer superlattice	Chalcopyrite	Layered Trigonal
Formula:	$n = 0,4; AC$	$n = 2; ABC_2$	$n = 1,3; A_3BC_4$	$n = 2; ABC_2$	$n = 2; ABC_2$	$n = 2; ABC_2$
						
Example: (ternary)	ZnS-type	InGaAs <sub>2</sub> -type (CA)	Cu <sub>3</sub> AsS <sub>4</sub> -type (L1 Or L3)	(AlGa) <sub>2</sub> (GaAs) <sub>2</sub> (Z2)	CuFeS <sub>2</sub> -type (CH)	CrCuS <sub>2</sub> -type (CP)
Bravais Lattice:	Face centered cubic	Simple tetragonal	Simple cubic	Simple tetragonal	Body centered tetragonal	Rhombohedral
Space Group	$F\bar{4}3m$	$P\bar{4}m2$	$P\bar{4}3m$	$P\bar{4}m2$	$I\bar{4}2d$	$R\bar{3}m$
Int. Tables:	$T_d^2$	$D_{2d}^5$	$T_d^1$	$D_{2d}^5$	$D_{2d}^{12}$	$C_{3v}^5$
Schoenflies:	$T_d$	$D_{2d}^5$	$T_d$	$D_{2d}^5$	$D_{2d}^{12}$	$C_{3v}$

FIG. 2. The crystal structures and their space-group notations (in the International Tables and Schoenflies conventions) for the special periodic structures used to obtain the interaction energies. In parentheses we give the abbreviated structure symbols (e.g., CA, CP, and CH) used in the text.